Cell Reports

Article

DOT1L/H3K79me2 represses HIV-1 reactivation via recruiting DCAF1

Graphical abstract

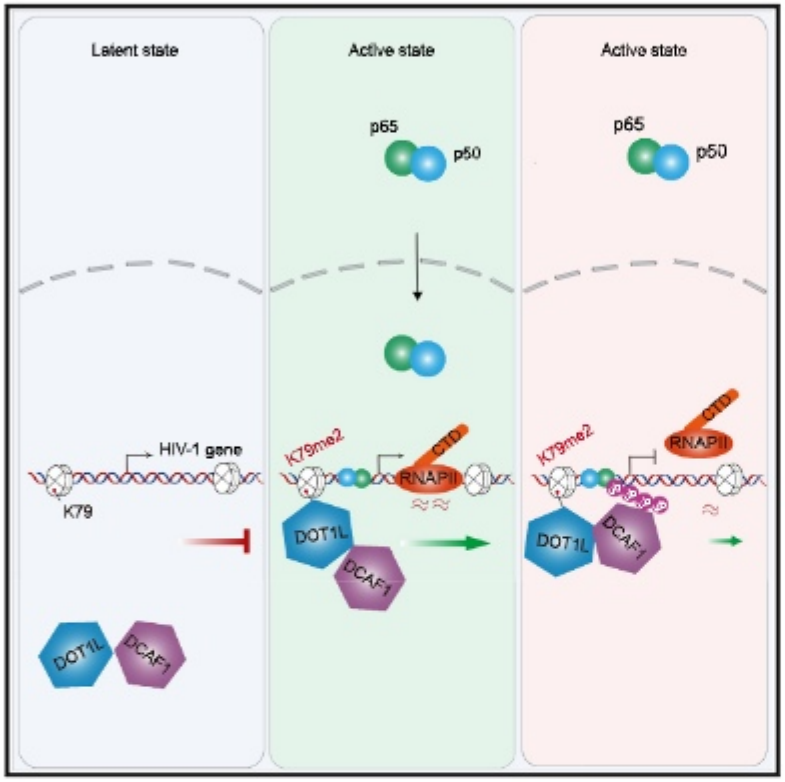

Highlights

- Peptide affinity purification identifies proteins recognizing methylated histone H3K79
- DCAF1 is associated with both H3K79me2 and DOT1L
- DOT1L/H3K79me2 facilitates recruitment of DCAF1 to constrain HIV-1 reactivation
- DCAF1 promotes ubiquitination of NF-κB and suppresses its level at HIV-1 LTR

Authors

Fenfei Liang, Jiaxing Jin, Qiming Li, ..., Yu Zhou, Deqing Hu, Liang Chen

Correspondence

hudq@tmu.edu.cn (D.H.), liang_chen@whu.edu.cn (L.C.)

In brief

Liang et al. demonstrated that DOT1L/H3K79me2, in conjunction with DCAF1, establishes a negative feedback loop to restrict HIV-1 reactivation by inhibiting NF-κB binding at LTR.

Liang et al., 2024, Cell Reports *43*, 114368
July 23, 2024
https://doi.org/10.1016/j.celrep.2024.114368

CellPress

Cell Reports

CellPress
OPEN ACCESS

Article

DOT1L/H3K79me2 represses HIV-1 reactivation via recruiting DCAF1

Fenfei Liang,[1] Jiaxing Jin,[2] Qiming Li,[1] Jiangkai Duan,[1] Ao Jiang,[1] Xiaoqing Chen,[1] Huichao Geng,[1] Kai Wu,[1] Fei Yu,[1] Xiaolu Zhao,[1] Yu Zhou,[1] Deqing Hu,[2,3,*] and Liang Chen[1,4,*]

[1]RNA Institute, Hubei Key Laboratory of Cell Homeostasis, College of Life Sciences, Wuhan University, Wuhan 430072, China

[2]State Key Laboratory of Experimental Hematology, Tianjin Key Laboratory of Medical Epigenetics, Tianjin Key Laboratory of Cellular Homeostasis and Human Diseases, Department of Cell Biology, School of Basic Medical Sciences, Tianjin Medical University, Tianjin 300070, China

[3]Key Laboratory of Breast Cancer Prevention and Therapy, Ministry of Education, Cancer Institute and Hospital of Tianjin Medical University, Tianjin 300060, China

[4]Lead contact

*Correspondence: hudq@tmu.edu.cn (D.H.), liang_chen@whu.edu.cn (L.C.)

https://doi.org/10.1016/j.celrep.2024.114368

SUMMARY

DOT1L mediates the methylation of histone H3 at lysine 79 and, in turn, the transcriptional activation or repression in a context-dependent manner, yet the regulatory mechanisms and functions of DOT1L/H3K79me remain to be fully explored. Following peptide affinity purification and proteomic analysis, we identified that DCAF1—a component of the E3 ligase complex involved in HIV regulation—is associated with H3K79me2 and DOT1L. Interestingly, blocking the expression or catalytic activity of DOT1L or repressing the expression of DCAF1 significantly enhances the tumor necrosis factor alpha (TNF-α)/nuclear factor κB (NF-κB)-induced reactivation of the latent HIV-1 genome. Mechanistically, upon TNF-α/NF-κB activation, DCAF1 is recruited to the HIV-1 long terminal repeat (LTR) by DOT1L and H3K79me2. Recruited DCAF1 subsequently induces the ubiquitination of NF-κB and restricts its accumulation at the HIV-1 LTR. Altogether, our findings reveal a feedback modulation of HIV reactivation by DOT1L-mediated histone modification regulation and highlight the potential of targeting the DOT1L/DCAF1 axis as a therapeutic strategy for HIV treatment.

INTRODUCTION

Epigenetics refers to the stable phenotypic changes that can be heritably transmitted without altering the DNA sequence. This regulatory process primarily involves molecular mechanisms at multiple levels, including DNA methylation, non-coding RNAs, and histone modifications. Among these mechanisms, histone methylation plays a crucial role in epigenetic regulation. It involves the covalent binding of specific amino acid residues (such as lysine and arginine) in histones to methyl groups under the action of methyltransferases. This modification alters the structure and stability of chromatin, thereby influencing gene expression.[1] In mammals, DOT1L (disruptor of telomeric silencing 1-like) is the sole methyltransferase that catalyzes the mono-, di-, and tri-methylation of H3K79.[2] Recent structural studies have elucidated the sequential events for methylation reaction at the molecular level: DOT1L is first recruited to the nucleosome, then immobilized via ubiquitinated H2BK120, and activated to mediate the methylation reaction on H3K79.[3–7] Specifically, after DOT1L forms a complex with the nucleosome, the ubiquitin on H2BK120, the acidic patch, and the H4 tail within the nucleosome restrict DOT1L's orientation. This positioning ensures that the active site of DOT1L faces toward the nucleosome and the H3K79 residue. On the other hand, however, the factors and mechanisms involved in removing or recognizing H3K79me, and downstream functions linked to the dynamic regulation of this epigenetic mark remain to be further explored.

DOT1L and H3K79me are frequently associated with active gene transcription.[8,9] They contribute to the maintenance of chromatin accessibility, histone acetylation, and the binding of specific transcription factors to promoters and enhancers, including H3K79me2/3 enhancer elements.[10] DOT1L may interact with the C-terminal domain of RNA polymerase II (RNAPII) and several RNAPII-associated elongation complexes.[11] In the context of MLL (mixed-lineage leukemia) -driven leukemia, DOT1L interacts with MLL translocation partner proteins within the super elongation complex. It drives gene expression through H3K79 methylation and contributes to disease progression.[12–14] Furthermore, DOT1L has been implicated in several other types of cancer, where it promotes gene activation.[15,16] Given these associations, DOT1L is a potential target for prognostic evaluation and therapeutic interventions.

Besides active gene loci, DOT1L and H3K79me play important roles in heterochromatic regions with repetitive DNA sequences as well, such as the telomere and centromere. Early studies have shown the presence of methylated H3K79 residues at the

heterochromatin territory.[17] In yeast, DOT1L was discovered to maintain telomere heterochromatin and gene silencing.[18] Such effect was later demonstrated to require Dot1 enzymatic activity and methylation at the H3K79 site.[19] In mouse embryonic stem cells, it has been demonstrated that DOT1L stimulates transcript production from the pericentromeric repeat regions, a process required for maintaining heterochromatin structure and genomic integrity.[20] Intriguingly, a recent report has unraveled that DOT1L controls the deposition of histone H1 variants via Npm1 to suppress the expression of endogenous retroviruses, such as MERVL (murine endogenous retrovirus-L).[21] Collectively, these findings indicate that DOT1L plays divergent roles in transcriptional regulation at genomic regions bound by distinct co-factors or H3K79me readers.

DOT1L/H3K79me is involved in viral infection as well. In herpes simplex virus type 1-infected herpes simplex keratitis, inhibition of DOT1L constrains corneal oxidative stress and inflammation induced by the p38 pathway.[22] DOT1L silencing or treatment with its catalytic inhibitor pinometostat (EPZ5676) enhances the replication of influenza and vesicular stomatitis viruses.[23] Further analysis has revealed that EPZ5676-treated cells display decreased nuclear translocation of the NF-κB complex and antiviral type I interferon response associated with increased viral replication.[23] Such an antiviral role of DOT1L was reported in studies of other viruses, such as the Sendai virus.[24] However, upon the infection of the avian leukosis virus, DOT1L may play an opposite role by restricting the innate immune response in host cells.[25] These results therefore reinforce the context-dependent functions of DOT1L in response to viral infection.

In this study, we performed the peptide affinity purification and mass spectrometry analysis in HEK293T cells to identify hundreds of proteins linked to the histone H3K79 residue in a methylation-specific manner. A component of the E3 ligase complex implicated in the HIV life cycle, DCAF1 (DDB1 and CUL4 associated factor 1), was further confirmed to be associated with H3K79me2 and DOT1L. We then examined the role of DOT1L/H3K79me and DCAF1 in HIV-1 provirus latency maintenance and reactivation induced by the TNFα/NF-κB pathway, and we identified DOT1L/H3K79me/DCAF1 axis negatively modulated HIV-1 reactivation. Furthermore, we examined the potential role of DCAF1 in controlling NF-κB occupancy at the HIV-1 long terminal repeat (LTR) region. Lastly, we combined the treatment of EPZ5676 and latency reversing agents (LRAs) in the HIV-1 latent cell model and demonstrated a synergistic effect on HIV-1 reactivation.

RESULTS

Identification of proteins associated with methylated H3K79 by mass spectrometry

While several protein factors have been linked to histone H3K79 methylation,[26–29] the regulation and functions of the DOT1L/H3K79me axis in different contexts remain incompletely understood. To identify candidate proteins that directly or indirectly bind to methylated H3K79, we conducted an *in vitro* biotin-labeled peptide pull-down assay followed by mass spectrometry analysis. Specifically, we synthesized four types of biotinylated, 22-amino acid (aa) peptides that mimic the protein sequence of histone H3 from aa 69 to 90. These peptides featured zero to three methyl groups at the K79 site. Additionally, we included a mixture of random 22-aa peptides as the control (Figure 1A). The peptides were mixed with streptavidin magnetic beads to form the peptide-bead conjugates, which were then incubated with nuclear lysates prepared from HEK293T cells (Figure 1B). Bound proteins were resolved through SDS-PAGE, visualized by silver staining, and analyzed via mass spectrometry (Figures 1C and S1A). In total, 590 proteins were significantly associated with at least one H3K79-containing peptide compared to the random control (Table S1).

Clustering analysis showed proteins identified by peptides with H3K79me0 and H3K79me1 largely overlapped ones pulled down by the peptide containing H3K79me2, suggesting these proteins bind to peptides *in vitro* depending on peptide sequence rather than the methyl group (Figure 1D). Besides these commonly associated factors, H3K79me2 was bound by a unique group of proteins, and so was H3K79me3 (Figures 1D and 1E), implicating the steric impact of multi-methyl groups on protein binding.[30,31] We then focused our analysis on these unique proteins, which were 224 for H3K79me2 and 169 for H3K79me3. Gene Ontology (GO) analysis has identified that H3K79me2-recognizing proteins are involved in the regulation of gene expression and metabolic process or components of the mediator complex, while many H3K79me3-associated proteins are implicated in RNA metabolic process or belong to the ribosomal protein complexes (Figure S1B). Of note, the protein interaction network analyses have uncovered that many proteins specifically associated with H3K79me2 were subunits of several transcription-regulating complexes, such as the mediator, integrator, NELF (negative elongation factor),[32] and CCR4-NOT complex[33] (Figure 1F). To verify the mass spectrometry results, we performed an *in vitro* pull-down assay followed by western blot to examine a few listed H3K79me2-binding proteins that function in transcription regulation, including MED23, NELFE, CBX8, CPSF6, CPSF3L, and INTS9. MEN1 (menin) was also included for validation as it is a direct binding protein of H3K79me2.[26] Indeed, the results confirmed that all tested proteins preferred to bind to H3K79me2 (Figure S1C). In sum, our data suggest that H3K79me2 associated with unique factors may participate in transcription regulation with various co-factors.

Interaction of DCAF1 with DOT1L

Several protein domains that recognize methylated lysine in histones have been reported, such as the PHD, WD40-repeat and ankyrin-repeat domain, and the Royal domain family. The Royal domain family includes the Tudor, Chromo, MBT, and PWWP domains.[34,35] To identify associated proteins that recognize H3K79me2/me3, we performed domain enrichment analysis and discovered two chromo domain-containing proteins, CHD8 and DCAF1 (also called VPRBP), specifically for H3K79me2 (Figures S2A and S2B). *In vitro* peptide pull-down assay further validated both proteins preferred to associate with the H3K79me2-containing peptide (Figure 2A).

We were intrigued by DCAF1, as it is a component of the E3 ubiquitin ligase implicated in transcriptional regulation,[36–38] but

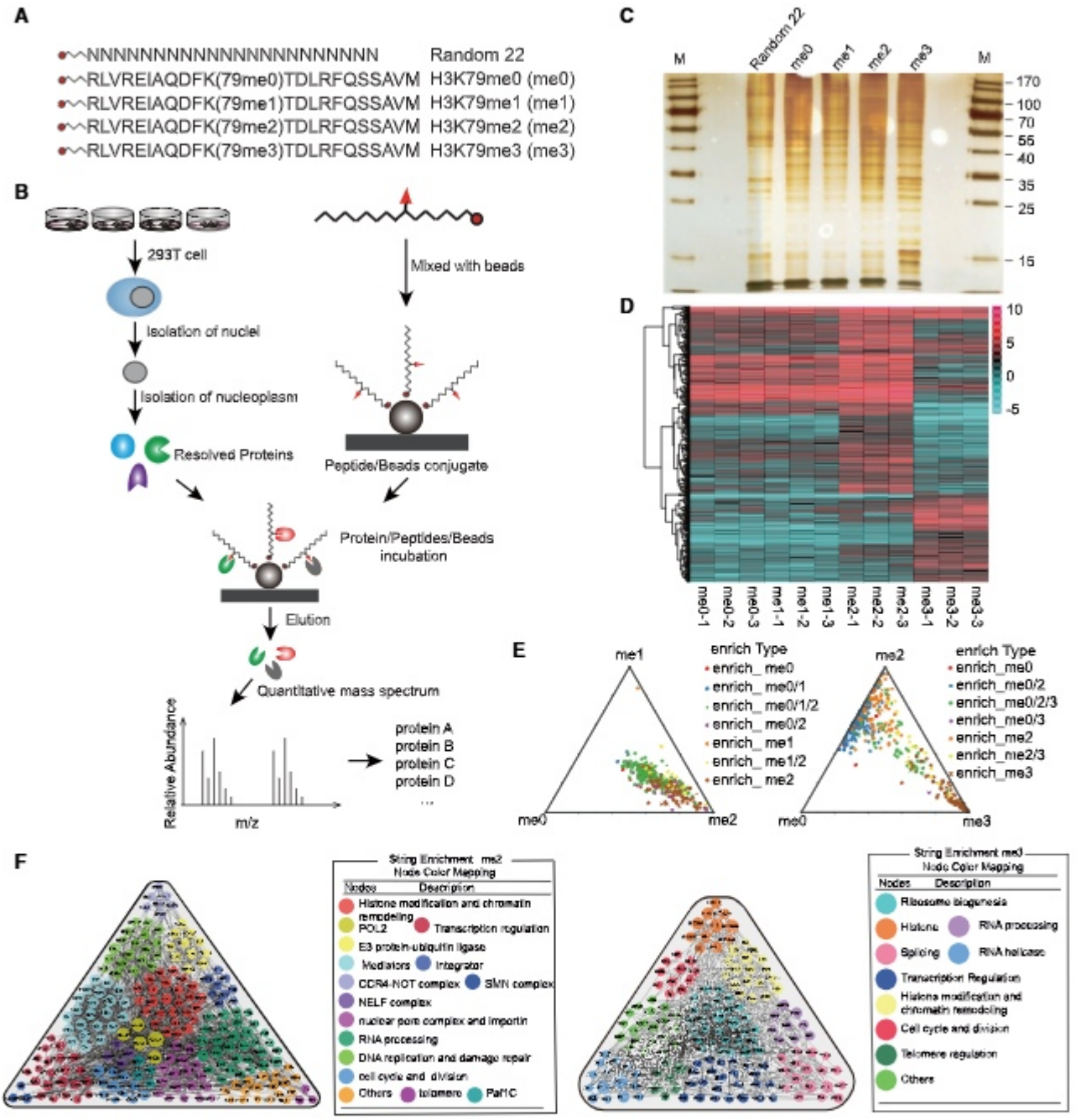

Figure 1. Mass spectrometry experiment design and capturing of H3K79 methylation-interacting proteins

(A) Design and synthesis of biotinylated peptides, including the 22-aa peptide mix of random sequences and ones mimicking H3 aa 69–90 with different numbers of methyl groups at K79.

(B) Schematics of the peptide pull-down assay.

(C) Visualization of factors associated with peptides in silver stain gel.

(D) Cluster and heatmap results for differential binding proteins. Each column represents a sample, with three replicates per sample, and each row represents an associated protein.

(E) The ternary diagram showing the preferred binding proteins to H3K79me0, me1, or me2 (left) and to H3K79me0, me2, or me3 (right). The color points represent proteins with different binding preferences (enrichment). Fold change ≥ 3 and the $p \leq 0.05$ are considered as significant enrichment.

(F) Interaction map of H3K79me2- and me3-associated protein complexes distinguished by colors. The analysis was performed by STRING. See also Figure S1 and Table S1.

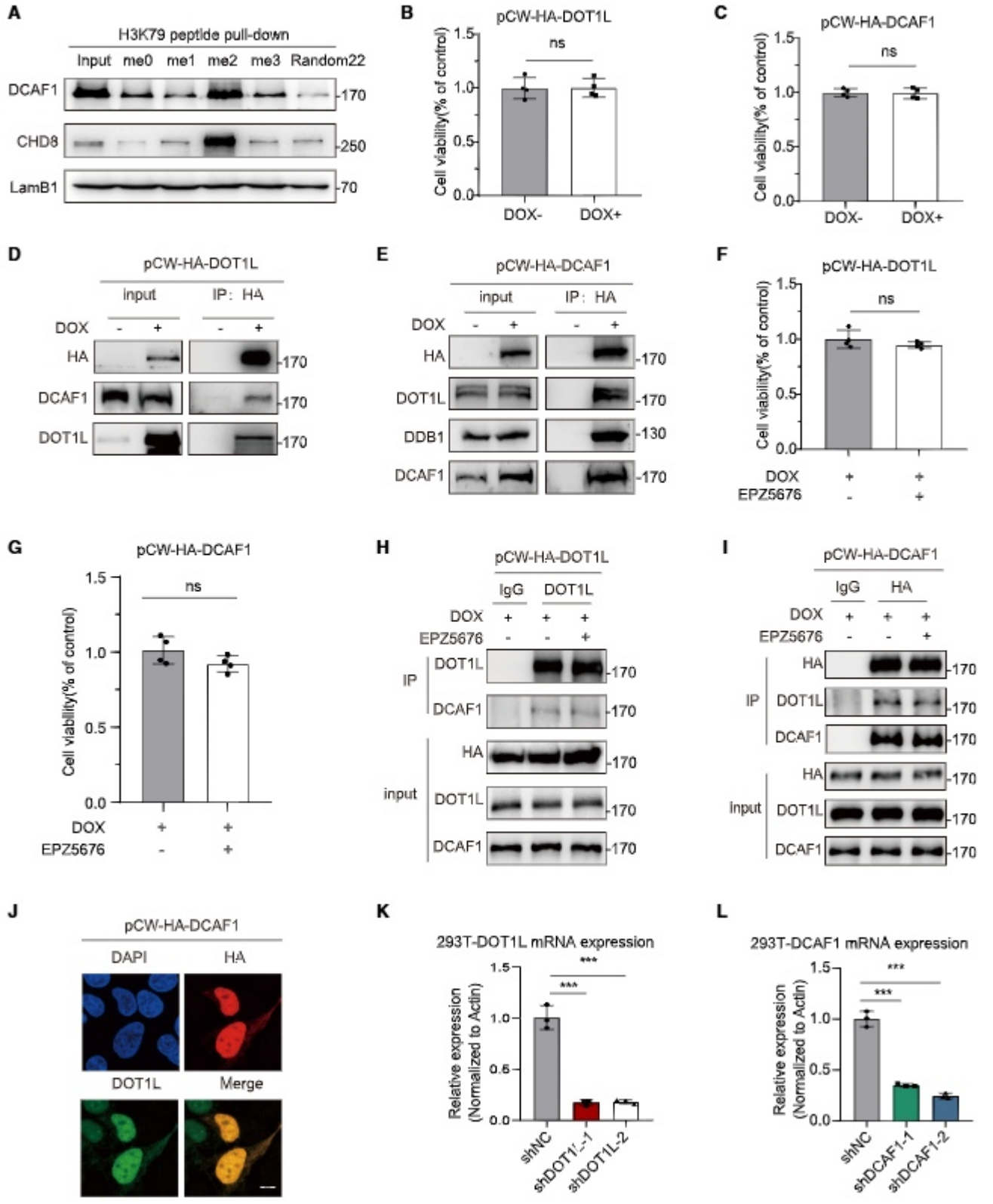

(legend on next page)

it has not been linked to DOT1L or H3K79me. To further explore the relationship between DCAF1 and the DOT1L/H3K79me regulatory axis, we constructed the doxycycline (DOX)-induced DOT1L- or DCAF1-expressing HEK293T cell lines (Figures S2C and S2D), the viability of which were not affected by DOX treatment (Figures 2B and 2C). We then conducted the reciprocal co-immunoprecipitation assays and found that DCAF1 could interact with DOT1L (Figures 2D and 2E). Interestingly, such association was unaffected in cells pretreated with EPZ5676, suggesting that DOT1L activity is not required for protein interaction (Figures 2F–2I). Furthermore, we performed the immunostaining experiment indicative of the co-localization of DOT1L and DCAF1 in the nucleus (Figure 2J).

To dissect the potential biological impacts of DOT1L interacting with DCAF1, we established the HEK293T cell lines expressing the small hairpin RNA (shRNA) to specifically target *DOT1L* or *DCAF1* for repression in a DOX-treatment-dependent manner. Both real-time qPCR and western blot showed that DOT1L and DCAF1 were significantly ablated by specific shRNAs induced by DOX, without compromising the cell viability (Figures 2K, 2L, and S2E–S2G). Furthermore, ablation of the expression or the enzymatic activity of DOT1L or repression of the expression of DCAF1 has little effect on the cell cycle progression (Figures S2, S2H, and S2I). Collectively, these results suggest neither DOT1L nor DCAF1 is essential for HEK293T cell growth.

Both DOT1L/H3K79me2 and DCAF1 repress latent HIV reactivation

Both DOT1L and DCAF1 are implicated in HIV life cycle control.[36,39,40] Our finding of the interaction between DOT1L/H3K79me2 and DCAF1 thereafter prompted us to examine if DOT1L and DCAF1 modulate certain stages of HIV life cycle in a coordinative manner. As both proteins are mainly in the nucleus and DOT1L functions on chromatin, we reasoned to focus our study on the HIV latency maintenance and reactivation. We used two latent cell models, E4 and 2D10, in which the modified HIV-1 genome was integrated into either the second exon of the *MSRB1* gene or the 11th intron of *CD2AP*. Moreover, a green fluorescent protein reporter gene has been inserted into the *nef* gene for monitoring the level of HIV-1 gene expression in both cell models.[41] The integrated HIV-1 genome in both cell lines can be activated by TNFα treatment or by the expression of the viral protein Tat.[41,42]

With these latent HIV-1 models, we constructed cell lines expressing shNC or shDOT1L in a DOX-induced manner and observed little defects in cell viability (Figure S3A). During the latency period, the proportion of GFP-positive cells remained the same in both E4 or 2D10 cells following DOT1L ablation (Figures 3A, 3B, S3B, and S3C). On the other side, however, the proportion of GFP-positive cells was significantly upregulated following TNFα treatment for 12 h and further elevated by the ablation of DOT1L expression in both cell lines. Accordingly, the expression of GFP protein was enhanced in shDOT1L-expressing cells compared to that in shNC control by western blot (Figure 3C). To determine if DOT1L functions through its enzymatic activity, we pretreated E4 and 2D10 cells with EPZ5676 followed by TNFα induction. Indeed, we found that removal of the H3K79me decoration further increased the percent of reactivated GFP-positive cells for both cell lines, without any effect on cell viability (Figures 3D–3F, S3D and S3E). Inspired by these findings, we generated the shDCAF1-expressing E4 cell lines and observed the same trends following the TNFα treatment as that for shDOT1L cells (Figures 3G–3I and S3F–S3I). Interestingly, when we simultaneously blocked DOT1L activity and DCAF1 expression by EPZ5676 treatment in shDCAF1-expressing E4 cells, no additive effect was observed in comparison to either treatment alone, suggesting that DOT1L and DCAF1 may function in the same axis in HIV-1 reactivation (Figures 3J–3L and S3I).

It has been shown that transcriptional reactivation of the HIV provirus genes would gradually be reversed to the latent state after TNFα is withdrawn.[42] To examine if DOT1L/H3K79me and DCAF1 are involved in the maintenance or reversal of the activation status, we treated cells with TNFα for 24 h and then replaced the stimulation with the regular medium. While the percentage of GFP-positive cells gradually returned to the basal level in 6 days, such a process was significantly delayed by suppressing the expression of *DOT1L* or *DCAF1* or by EPZ5676 treatment (Figures 3M–3O and S3J–S3L). In sum, our data indicate that DOT1L plays a negative role via its enzymatic activity, possibly together with DCAF1, in induced HIV-1 activation and maintenance.

Transcriptome alteration following DOT1L inhibition and HIV-1 reactivation

DOT1L is primarily suggested as a positive regulator of transcription, which contrasts with our observations in HIV-1 reactivation, raising a question as to whether DOT1L modulates HIV-1 reactivation directly or indirectly. To tackle this question, we began to characterize the impact of DOT1L activity on transcriptome

Figure 2. Interaction of DCAF1 with DOT1L and H3K79me2

(A) Verification of DCAF1 and CHD8 by peptide pull-down and western blot. Random peptide 22 was used as a non-specific peptide and LamB1 as a non-specific binding protein.

(B and C) Cell viability examination by CCK8 assays for HEK293T cells overexpressing DOT1L (B) and DCAF1 (C). Data are presented as means ± SD ($n = 4$). Statistical significance was determined by the Student's t test. ns: no significance.

(D) Immunoprecipitation of HA-DOT1L from the HEK293T cell lysate followed by the western blot assay.

(E) Immunoprecipitation of HA-DCAF1 from the HEK293T cell lysate followed by the western blot assay.

(F and G) Cell viability examination by CCK8 assays for HEK293T cells overexpressing HA-DOT1L (F) and HA-DCAF1 (G), following the EPZ5676 treatment (1 μM).

(H and I) Immunoprecipitation of HA-DOT1L (H) and HA-DCAF1 (I) from the HEK293T cells expressing corresponding proteins with or without the EPZ5676 treatment followed by the western blot assay.

(J) Immunostaining of HA-DCAF1 (red), DOT1L (green), and DAPI (blue) in HEK293T cells exogenously expressing HA-DCAF1. Scale bar: 7.5 μm.

(K and L) Relative mRNA expression levels of endogenous DOT1L (K) and DCAF1 (L) in HEK293T cells expressing shDOT1L or shDCAF1. shNC: the cells expressing the scramble shRNA. Statistical significance was determined by the Student's t test, $^{***}p \leq 0.001$. See also Figure S2.

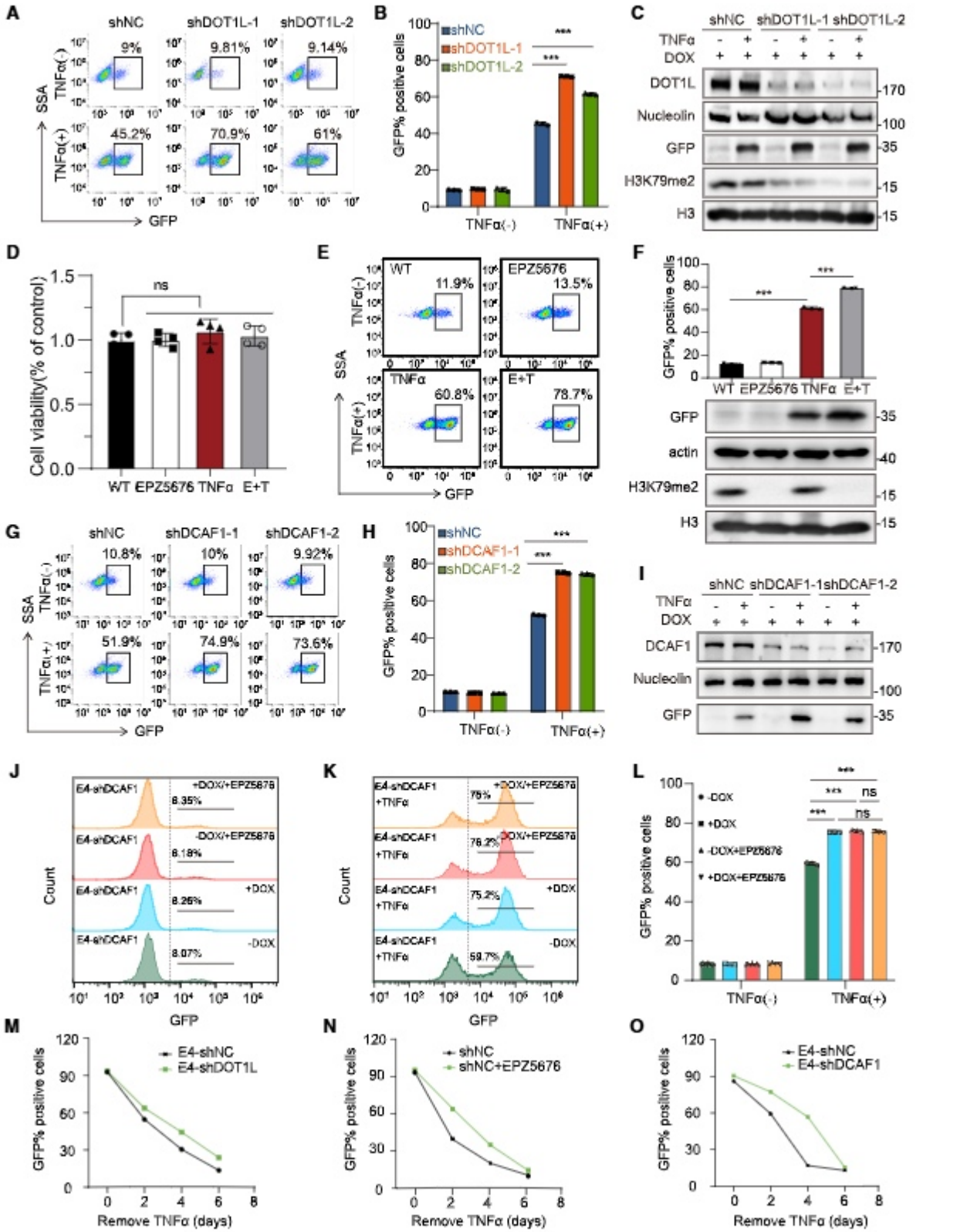

(legend on next page)

alterations by performing the RNA-seq analyses in E4 cells following the treatment of EPZ5676 (72 h), TNFα (12 h), or both. Notably, highly reproducible datasets indicated that incubation with TNFα elevated the expression of only a few genes (Figures 4A and S4A). A similar result was obtained from cells with dual treatments compared to that with EPZ5676 alone (Figure S4B). Meanwhile, there was little change in the expression of genes involved in gene set enrichment analysis enrichment categories related to TNFα signaling via NF-κB and inflammatory response (Figures 4B and 4C). This result is consistent with the established feedback mechanism, by which NF-κB activation is quickly turned down by induced expression of the inhibitory factor IκBα.[43,44] Taken together, the long-term (12 h) promotion of HIV-1 reactivation by DOT1L loss is not because of globally prolonged TNFα/NF-κB activation.

Treatment of cells with EPZ5676 led to significant upregulation of 389 genes and downregulation of 26 genes compared to untreated cells (Figure S4C). In parallel, dual treatments caused 385 upregulated and 40 downregulated genes compared to TNFα treatment alone (Figure S4D). Interestingly, the clustering analysis of differentially expressed genes revealed a large degree of overlap between datasets with EPZ5676 and dual treatments (Figure 4A, C1 and C2). Moreover, dual treatment changed the expression of only a few genes compared to EPZ5676 (Figure S4D). We validated several up- (C1) and downregulated (C2) genes by the real-time qPCR assays (Figures S4, S4E, and S4F). These results suggest that inhibition of DOT1L activity, but not long-term TNFα treatment, has a dominant influence on altered genes.

GO analysis showed genes in C1 were enriched in diverse developmental processes unrelated to the identity of E4 Jurkat cells (Figure S4G). In contrast, most of the terms for C2 were related to leukocyte-mediated cytotoxicity, lymphocyte-mediated immunity, and positive regulation of cell killing, consistent with the T lymphocyte origin of E4 cells (Figure S4H). These observations reminded us of previous reports that loss of DOT1L causes non-specific induction of silenced or inactive genes, where there is an absence of H3K79me decoration.[45] We thereafter compared the overall expression levels of upregulated, downregulated, and all genes in the presence of EPZ5676 treatment, the result of which showed that upregulated genes were indeed expressed at significantly lower levels than the downregulated and all-gene groups, consistent with their non-specific identifies to E4 cells (Figure S4I). As EPZ5676 alone induces the expression of C1 genes and dual treatments confer no additional effect (Figure 4A), we conclude that the enhancement of the HIV-1 reactivation by DOT1L inhibition is due to a mechanism different from that for C1 gene induction.

To examine if loss of DOT1L promotes HIV-1 reactivation through transcription, we calculated the expression of the HIV genome-encoded genes from the RNA-seq data. Similar to the results of GFP protein measurement, the expression of viral RNAs was significantly induced by TNFα, and the synergistic elevation was achieved by EPZ5676 pretreatment (Figure 4D). Real-time qPCR was conducted and further validated the RNA-seq results (Figure 4E). Intriguingly, C3 genes in host cells appeared to be regulated similarly to the HIV-1 genes, remaining silenced in the presence of EPZ5676, yet activated by TNFα and further induced by dual treatments (Figures 4A and 4F). GO analysis showed enriched terms in the immune response pathways (Figure S4J). Altogether, these data confirmed that DOT1L restrains TNFα-induced transcription of the HIV-1 genome-encoded genes, together with specific host genes.

DOT1L promotes the recruitment of DCAF1 to the HIV-1 LTR on chromatin

We next sought to examine if DOT1L directly regulates the transcription of HIV-1 genes upon reactivation. Chromatin immunoprecipitation (ChIP)-qPCR experiments were then performed to evaluate the levels of DOT1L and H3K79me2 at different positions of the HIV-1 LTR and the downstream integrated EGFP locus (Figure 5A). An H3 ChIP-qPCR was performed as the background control (Figures 5B, 5C, and S5A). While low in the latent stage, increased DOT1L occupancy and H3K79me2 level were observed upon TNFα stimulation, yet the H3 level that represents the nucleosome occupancy on chromatin remained unchanged (Figures 5B, 5C, and S5A). In particular, the most evident enhancement of DOT1L binding occurred at the HIV-1 LTR, whereas H3K79me2 marks were extended from the LTR to the downstream GFP region, suggesting that TNFα

Figure 3. DOT1L/H3K79me2 and DCAF1 repress the latent HIV-1 reactivation

(A) Flow cytometry analysis of two shDOT1L-expressing E4 cell lines at latency (TNFα−) and reactivation (TNFα+, 10 ng/mL, 12 h). Representative results of three technical repeats from at least three experiments were shown.

(B) Quantification of GFP-positive E4 cells expressing shNC or shDOT1L at latent stage or reactivated upon TNFα treatment. Data are presented as means ± SD ($n = 3$).

(C) The protein levels of DOT1L and GFP examined by western blot in E4 cells expressing shDOT1L with and without TNFα treatment. H3 was used as a control for H3K79me2.

(D) Cell viability examination by CCK8 assays for E4 cells treated with EPZ5676 and TNFα. Data are presented as means ± SD ($n = 4$). The statistical significance was determined by the Student's t test. ns: no significance.

(E and F) The flow cytometry analysis of E4 cell lines before and after the treatment of EPZ5676 and TNFα. Representative results of three technical repeats from at least three experiments. (E) The quantification of the flow cytometry assay (means ± SD; $n = 3$) and the western blot assay detecting the protein levels of GFP and H3K79me2 (F) are shown.

(G–I) The flow cytometry analysis of two shDCAF1-expressing E4 cell lines with or without TNFα treatment. Representative results are of three technical repeats from at least three experiments. (G) The quantification of the flow cytometry assay (means ± SD; $n = 3$) (H) and the western blot assay detecting the protein levels of GFP and DCAF1 (I) are shown.

(J and K) The flow cytometry analysis of the shDCAF1-expressing E4 cell line treated with EPZ5676 for 3 days without (J) or with (K) TNFα activation.

(L) The quantification of GFP-positive cells for (J) and (K). Data are presented as means ± SD ($n = 3$).

(M–O) The percentage of GFP-positive E4 cells expressing shDOT1L (M), treated with EPZ5676 (N), or expressing shDCAF1 (O). Cells were activated by TNFα for 24 h, which was replaced with fresh medium. ***$p \leq 0.001$. See also Figure S3.

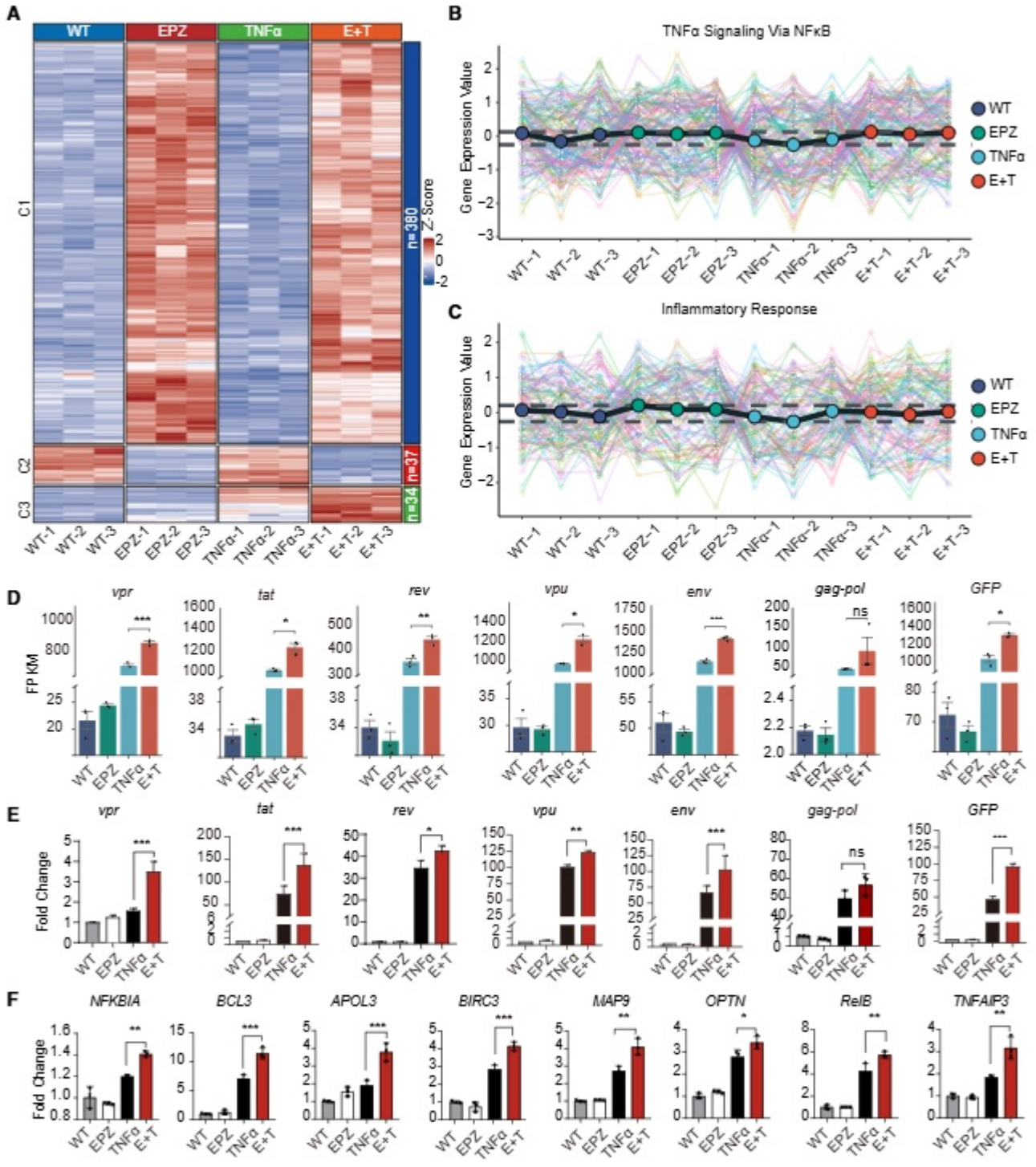

Figure 4. Transcriptome analysis following EPZ5676 treatment and HIV-1 reactivation

(A) Heatmap presentation of the differentially expressed genes identified by RNA-seq ($n = 3$) and organized by k-means clustering segmentation. EPZ: EPZ5676, E+T: EPZ5676 and TNFα.

(B and C) Expression alterations for gene sets involved in TNFα signaling via NF-κB pathway (B) and inflammatory response (C).

(D) Expression of HIV-1 genes by RNA-seq data. Data are presented as means ± SD ($n = 3$). FPKM: fragments per kilobase of transcript per million fragments.

(E) Real-time qPCR validation of HIV-1 gene expression by RNA-seq. Data are presented as means ± SD ($n = 3$).

(F) Real-time qPCR validation of the expression of C3 cluster genes by RNA-seq data. Data are presented as means ± SD ($n = 3$). $^{*}p \leq 0.05$, $^{**}p \leq 0.01$, and $^{***}p \leq 0.001$. See also Figure S4.

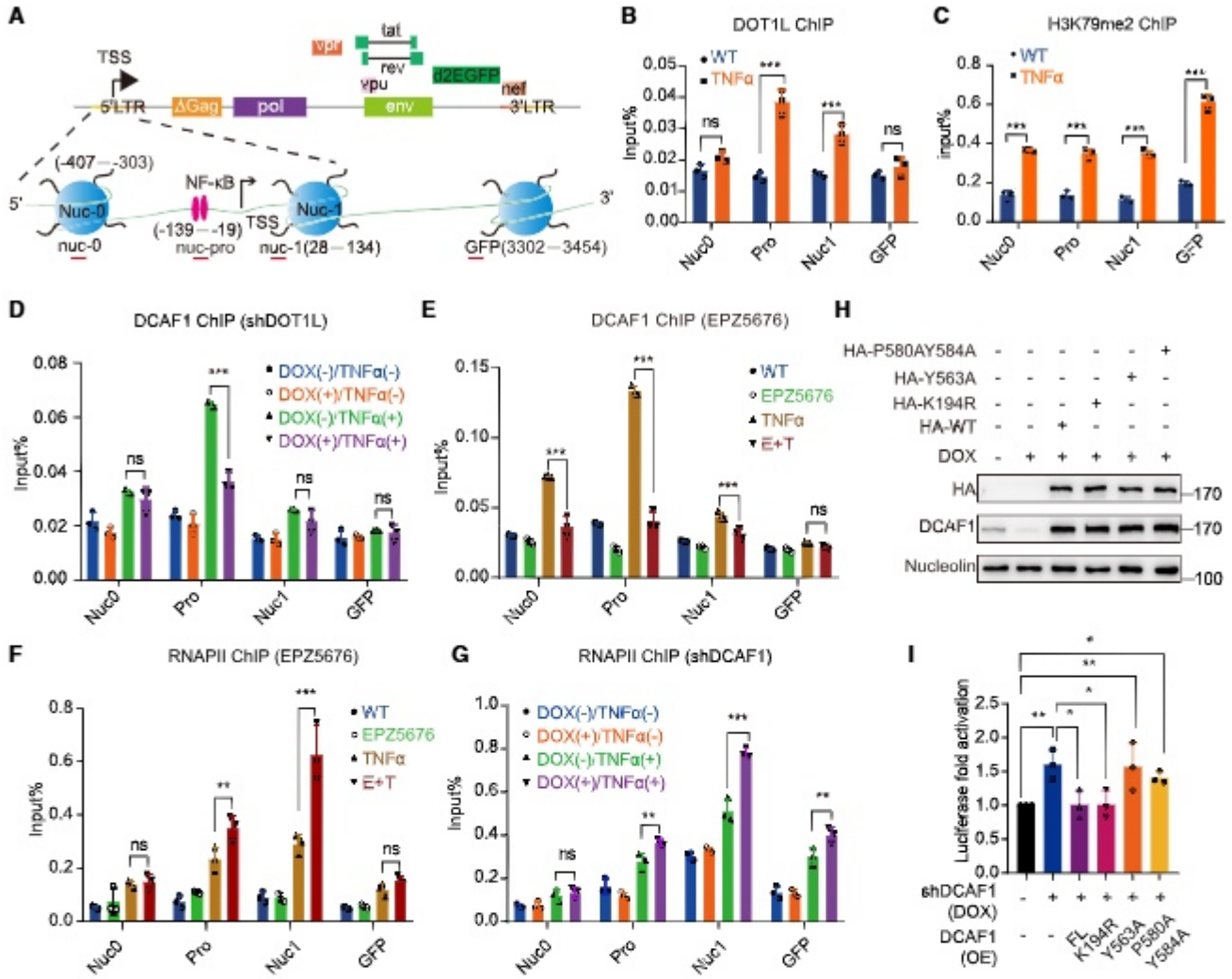

Figure 5. DOT1L promotes recruitment of DCAF1 to HIV-1 LTR

(A) Diagram of the HIV-1 genome and locations of primer pairs used in the ChIP-qPCR analyses. TSS, transcription start site. Pro, promoter. Nuc, nucleosome.

(B and C) ChIP-qPCR results showing the levels of DOT1L and H3K79me2 at HIV-1 LTR and downstream GFP regions in E4 cells following TNFα treatment for 12 h. ChIP enrichment values were normalized to input and are shown as means ± SD ($n = 3$).

(D and E) ChIP-qPCR results of DCAF1 occupancy at HIV-1 LTR and downstream GFP regions in E4 cells expressing shDOT1L and treated with or without TNFα for 12 h (D) and in cells treated with EPZ5676, TNFα, or both (E). Data were normalized to input and are shown as means ± SD ($n = 3$).

(F and G) ChIP-qPCR results of total RNAPII distribution at HIV-1 LTR and downstream GFP regions in E4 cells treated with EPZ5676, TNFα, or both (F) and in cells expressing shDCAF1 with or without TNFα treatment (G). Data were normalized to input and are shown as means ± SD ($n = 3$).

(H) The western blot assay examining the exogenous wild-type or mutant forms of HA-DCAF1 in HEK293T cells expressing shDCAF1.

(I) Dual luciferase assay results showing the transcription level of HIV-1 LTR in cells expressing shDCAF1 and the wild-type or mutant forms of DCAF1. The luciferase activity in each type of cell was normalized to the Renilla activity and presented as fold change compared to untreated wild-type cells. Data are expressed as mean ± SD ($n = 3$). FL: full-length wild type. *$p \leq 0.05$, **$p \leq 0.01$, and ***$p \leq 0.001$. ns: not significant. See also Figure S5 and Table S3.

induces the binding of DOT1L to the HIV-1 LTR, where it conducts methylation of the downstream nucleosomes.

We next asked if DCAF1 is recruited to the HIV-1 LTR in a DOT1L/H3K79me2-dependent manner or vice versa. By ChIP-qPCR assays, we observed that DCAF1 occupancy at the LTR and GFP loci were low during the latent state and remained unchanged in *DOT1L*-deficient cells or following EPZ5676 treatment (Figures 5D and 5E). Upon TNFα stimulation, however, a significantly higher level of DCAF1 was recruited to the HIV-1 promoter, which was reversed by ablation of the expression or the enzymatic activity of DOT1L (Figures 5D and 5E). In contrast, the induced chromatin binding of DOT1L seemed to be unaffected by blocking the expression of DCAF1 (Figure S5B). In sum, these results indicate that TNFα induces the binding of DOT1L to the HIV-1 LTR, which mediates the methylation of H3K79 and endorses the recruitment of DCAF1.

We then explored how DOT1L and DCAF1 may modulate the activity of total RNAPII. The ChIP-qPCR results showed that the

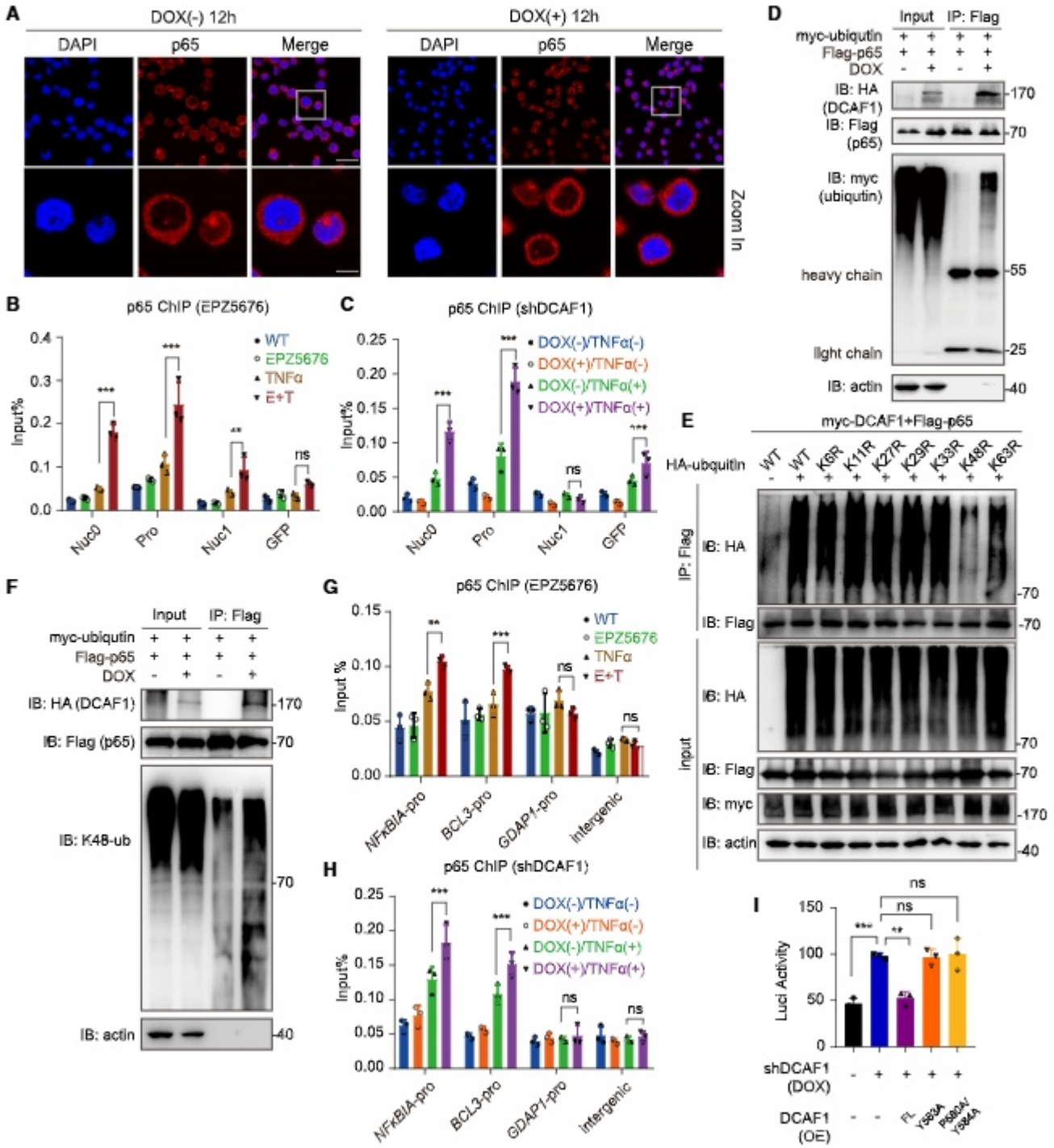

Figure 6. DCAF1 mediates the ubiquitination of p65 and constrains its binding at the HIV-1 LTR

(A) Immunofluorescence staining results of p65 in E4 cells expressing shDCAF1 with or without TNFα treatment for 12 h (up) and representative zoom-in area from the rectangle. Scale bar: 25 μm (up); scale bar: 7.5 μm (down). DAPI (blue); p65 (red).

(B and C) ChIP-qPCR results of p65 binding at the HIV-1 LTR and downstream GFP gene in E4 cells pretreated with EPZ5676 (B) or expressing shDCAF1 (C) followed by TNFα activation. Data were normalized to input and are shown as means ± SD ($n = 3$).

(D) Immunoprecipitation of FLAG-p65 in HEK293T cells overexpressing HA-DCAF1, FLAG-p65, and myc-ubiquitin, followed by western blot to examine the ubiquitination level of FLAG-p6.

(E) Immunoprecipitation of FLAG-p65 in HEK293T cells overexpressing myc-DCAF1, FLAG-p65, and HA-ubiquitin (wild type and mutants), followed by western blot to examine the ubiquitination level of FLAG-p65.

(legend continued on next page)

occupancy of RNAPII at the promoter and downstream coding region was significantly increased by TNFα treatment, suggesting both the transcriptional initiation and elongation are induced for the production of viral RNAs (Figures 5F and 5G). Importantly, EPZ5676 treatment and suppression of DCAF1 expression further enhanced TNFα induced RNAPII binding. Together with the increased expression level of HIV genes (Figures 4D and 4E), the induced RNAPII profile may be attributed to a rise in total RNAPII levels at these specific sites yet less likely to the shift of RNAPII from an elongated to a paused state following DOT1L inhibition. Such an antagonistic role of the DOT1L/H3K79me2/DCAF1 axis in RNAPII activity at HIV-1 LTR against TNFα mechanistically differs from the role of DOT1L in leukemia.

Besides working as a component of the E3 ubiquitin ligase complex, DCAF1 has been reported to harbor a kinase domain, the function of which is implicated in transcription repression by phosphorylating histone H2A at the T120 site.[46] To explore the mechanism of DCAF1 on HIV-1 transcriptional modulation in more detail, an HIV luciferase reporter system was introduced into HEK293T cells (see STAR Methods). In line with the above results, depletion of *DOT1L* or *DCAF1* expression following transfection of either small interfering RNA (siRNA) or shRNA significantly promoted Tat-induced HIV-1 reactivation (Figures S5C–S5E). We then generated several mutant DCAF1 expression vectors, including the K194R kinase-dead mutant[46] and Y563A and P580A/Y584A mutant forms that lack the methyl residual binding activity of the chromo domain in DCAF1,[31] and we introduced them into shDCAF1-expressing cells (Figures 5H and S5F). While exogenous expression of the full-length DCAF1 completely reversed the induced luciferase expression to the level seen in wild-type cells, two chromo domain mutant proteins failed to do so, suggesting the association of DCAF1 with H3K79me is necessary for antagonizing HIV-1 reactivation. (Figure 5I). In contrast, expression of the K194R kinase-dead mutant reversed the induced luciferase activation to a level similar to that in cells expressing the full-length DCAF1, therefore suggesting the kinase activity is not required for DCAF1 to modulate the transcription of HIV-1 genes (Figure 5I).

DCAF1 constrains the NF-κB level at the LTR binding sites

It has been reported that DCAF1 negatively regulates cellular immune responses by preventing nuclear translocation of NF-κB after activation.[47] We tested this possibility by carefully examining the directed relocation of p65, a subunit of the NF-κB dimer, in cells with or without DCAF1 expression. The amount of p65 in the nucleus was significantly increased as early as 0.5 to 1 h following TNFα treatment. The majority of nuclear p65 returned to cytosol at 12 h post treatment (Figures 6A and S6B). Importantly, no difference in the cytosol/nucleus distribution of p65 in cells with or without DCAF1 expression was observed at each time point, therefore excluding the possible impact of DCAF1 on HIV-1 reactivation by mediating NF-κB nuclear translocation (Figures 6A, S6A, and S6B).

As the NF-κB dimer is known to bind to the HIV LTR and activate gene expression,[48] we next measured the abundance of p65 at the annotated NF-κB binding sites within the LTR region, which was indeed upregulated following TNFα stimulation and further enhanced by EPZ5676 treatment (Figure 6B). Meanwhile, we observed similar results in shDCAF1-expressing cells (Figure 6C). These data suggest that DOT1L/DCAF1 counteracts the HIV-1 reactivation by reducing the level of NF-κB at LTR (Figure 6C). We then sought to test if DCAF1 regulates p65 by increasing its ubiquitination level. To do so, the myc-tagged ubiquitin and FLAG-tagged p65 expression vectors were transfected into HEK293T cells that express HA-DCAF1 via DOX induction. The immunoprecipitation assay was performed to show that DCAF1 interacts with p65 (Figure 6D). Moreover, the ubiquitination level of immunoprecipitated p65 was markedly increased in cells overexpressing DCAF1. To determine the ubiquitin-linkage specificity, we transfected HEK293T cells with myc-DCAF1, FLAG-p65, and HA-tagged wild-type ubiquitin or one of its variants with a single lysine-arginine substitution at one of seven lysine residues, namely, K6R, K11R, K27R, K29R, K33R, K48R, and K63R. Following the immunoprecipitation with the FLAG antibody, we observed that K48R mutation caused a significant loss of polyubiquitinated p65 signals, suggesting that p65 ubiquitination mainly involves K48-linked polyubiquitin chains (Figure 6E). In accordance, we co-transfected HEK293T cells overexpressing HA-DCAF1 with the myc-ubiquitin and FLAG-p65 expression vectors. Immunoprecipitation with an anti-FLAG antibody followed by western blot assay with an anti-ubiquitin K48 antibody further confirmed that p65 was linked to ubiquitin by K48 lysine residues (Figure 6F). In sum, our data suggest that DCAF1 functions to reduce the abundance of NF-κB at the viral promoters, possibly by mediating the ubiquitination of NF-κB.

Given the combinatorial effects of TNFα and EPZ5676 on the induction of C3 host gene (Figure 4F), we were next interested in determining if the DOT1L/DCAF1/NF-κB regulatory axis we dissected is applied to C3 genes as well. To do so, we screened the promoter of all C3 genes and found that 24 out of 34 (70.6%) contain the NF-κB binding sites (Figure S6C; Table S2). By further filtering with the NF-κB target genes database (https://esbl.nhlbi.nih.gov/Signaling-Pathways/NF-kB-Targets/), five C3

(F) Immunoprecipitation of FLAG-p65 in HEK293T cells overexpressing HA-DCAF1, FLAG-p65, and myc-ubiquitin, followed by western blot to examine the K48 ubiquitination level of FLAG-p65.

(G and H) ChIP-qPCR results of p65 binding at promoters of two NF-κB target genes from C3 in E4 cells pretreated with EPZ5676 (G) or expressing shDCAF1 (H) followed by TNFα activation. The promoter of GDAP1 and a randomly picked intergenic region were included as non-specific controls. Data were normalized to input and are shown as means ± SD ($n = 3$).

(I) Dual luciferase assay results showing the NF-κB-luc activity of HEK293T cells expressing shDCAF1 and complemented with overexpressed wild-type or mutant forms of DCAF1. The firefly luciferase activity representing the NF-κB-luc activity was measured and normalized to Renilla. Data are presented as mean ± SD ($n = 3$). FL: full-length wild type; Y563A, P580A/Y584A: two chromo domain mutant forms of DCAF1. $^{*}p \leq 0.05$, $^{**}p \leq 0.01$, and $^{***}p \leq 0.001$. See also Figure S6 and Tables S2 and S3.

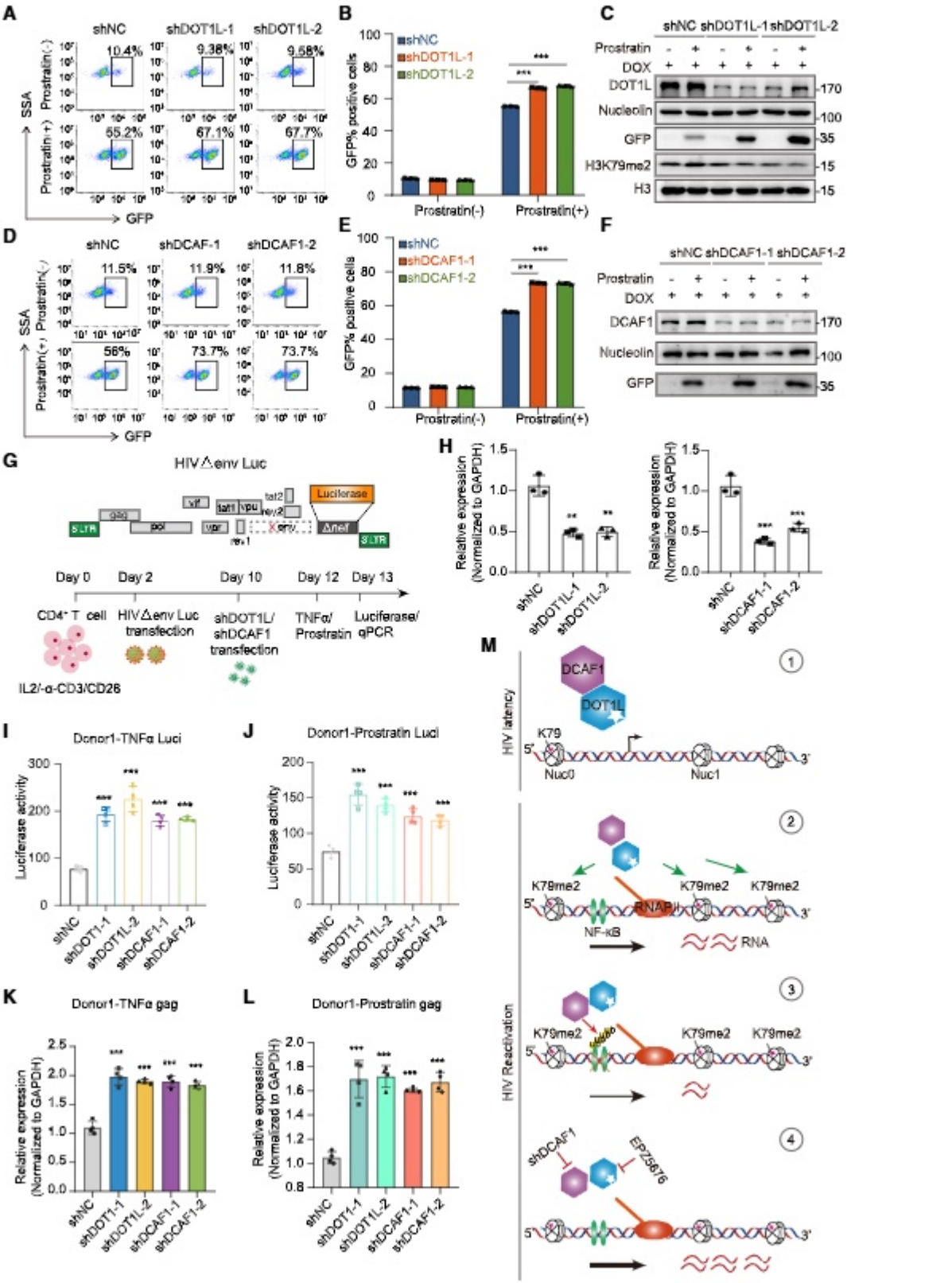

(legend on next page)

genes were identified as known NF-κB target genes, namely *LTB*, *TNFAIP3*, *NFKBIA*, *BCL3*, and *RELB*. We selected *NFKBIA*, *BCL3*, *GDAP1* (a non-target gene), and an intergenic region for the following study (Figure S6C).

In line with our findings at the HIV-1 LTR, the binding of DOT1L to the promoter of *NFKBI1* and *BCL3* was induced upon TNFα treatment, yet no change was seen at the *GDAP1*-pro and intergenic region (Figure S6D). Although the association of DCAF1 with the promoter of *NFKBI1* and *BCL3* was substantially increased by TNFα treatment, it was completely reversed by the ablation of DOT1L expression or its enzymatic activity (Figures S6, S6E, and S6F). Accordingly, TNFα-induced binding of p65 at two C3 genes was further elevated by the treatment of EPZ5676 or the ablation of DCAF1 expression (Figures 6G and 6H). To further examine if DCAF1 modulates the activity of NF-κB on chromatin, we examined the NF-κB luciferase activity in cells and indeed observed that knockdown of *DCAF1* promoted TNFα induced reporter activity, which could be fully reversed by exogenously supplementing wild-type but not the chromo domain mutant form of DCAF1 (Figure 6I). Consequently, the recruitment of RNAPII to *NFKBI1* and *BCL3* promoters, but not to non-target and intergenic regions, was significantly induced by TNFα in DCAF1 knockdown cells (Figure S6G). These data suggest that DOT1L/DCAF1 axis plays similar regulatory roles in NF-κB regulation at a subset of target genes in host cells (see discussion).

DOT1L and DCAF1 repress the reactivation of HIV-1 upon LRA treatment

One of the prevailing challenges in treating AIDS is the latency form of HIV provirus that leads to persistent HIV reservoir.[49,50] Various strategies have been proposed to eliminate latent HIV-containing cells, including the "shock and kill" method that uses LRAs to awaken the latent reservoir for the immune system to recognize and eliminate the virus-containing cells.[49,51] We next tested if EPZ5676 treatment leads to a synergistic effect with existing LRAs on the "shock" step. Two widely tested LRAs were tested in our study, including a PKC activator called prostratin that activates the NF-kB pathway[52] and bromodomain inhibitor called JQ1.[53] Consistent with the above tests by TNFα, treatment of prostratin significantly increased the number of GFP-positive cells, which was further enhanced by DOX-induced ablation of DOT1L expression (Figures 7A–7C). Knockdown of DCAF1 gave rise to the same trend in induced GFP expression (Figures 7D–7F). Meanwhile, we combined EPZ5676 and prostratin and found that the number of GFP cells was significantly upregulated, too (Figures S7A and S7B). We applied the JQ1 treatment to shDOT1L- or shDCAF1-expressing cells, and we observed similar synergistic effects (Figures S7C–S7F). These results together suggest that DOT1L and DCAF1 may be targeted together with currently used LRAs for synergistic HIV-1 reactivation.

To evaluate the role of DOT1L and DCAF1 in regulating HIV-1 reactivation with more clinical relevance, we infected $CD4^+$ T cells isolated from PBMC cells of two healthy donors with the HIV-1 luciferase reporter viruses (Figure 7G). After the cells returned to the resting period, they were infected with shDOT1L and shDCAF1 viruses (Figure 7H) and activated by either TNFα or prostratin. The results of the luciferase activity assay showed that depletion of either *DOT1L* or *DCAF1* markedly enhanced the HIV-1 reactivation level compared with the shNC control group (Figures 7I, 7J, S7G, and S7H). The real-time qPCR examination on the expression of the HIV-1 gag gene further confirmed the luciferase assay results (Figures 7K, 7L, S7I, and S7J). In sum, these data with primary $CD4^+$ T cells suggest that DOT1L and DCAF1 are two potential targets of new therapy designs for HIV patients.

DISCUSSION

The challenge in identifying factors associated with H3K79me is that this residue is embedded in the nucleosome core region. Potential binding proteins and readers may need special structural fitness or assistance from other factors to recognize this region.[21,27] It was recently reported that nucleosome assembly followed by pull-down assay well mimics the natural condition for identifying genuine binding proteins.[26] On the other hand, our strategy of using peptides containing H3K79 residue with various methyl groups can maximally differentiate the binding preference for each methyl group and cancel non-specifically associated proteins from the assay.

Indeed, the inclusion of known H3K79me-associated proteins, such as CBX8, NELFE, and MEN1, in our data supports the

Figure 7. DOT1L and DCAF1 repress the reactivation of HIV-1 upon LRA treatment

(A–C) Flow cytometry results showing percentages of GFP-positive E4 cells expressing shNC, shDOT1L-1, or shDOT1L-2, respectively, at latency or upon reactivation by prostratin treatment (1 μM, 16 h) (A). Quantification of GFP-positive cells is presented as means ± SD ($n = 3$) (B), and the protein levels of DOT1L and GFP were examined by western blot (C). H3 was used as a control for H3K79me2. Representative results of three technical repeats from at least three reproducible experiments are shown for (A) and (B).

(D–F) Flow cytometry results showing percentages of GFP-positive E4 cells expressing shNC, shDCAF1-1, or shDCAF1-2, respectively, at latency or upon reactivation by prostratin treatment (D). Quantification of GFP-positive cells is presented as means ± SD ($n = 3$) (E), and the protein levels of DCAF1 and GFP were examined by western blot (F). Representative results of three technical repeats from at least three reproducible experiments are shown for (D) and (E).

(G) Schematic representation of HIV-1_{NL4-3} luciferase reporter and experimental procedure for primary $CD4^+$ T cells from healthy donors followed by TNFα/prostratin reactivation.

(H) Real-time qPCR validation of DOT1L and DCAF1 gene expression in primary $CD4^+$ T cells expressing shDOT1L or shDCAF1.

(I and J) Luciferase activity detected upon TNFα (I) or prostratin (J) activation in $CD4^+$ HIV-1-infected cells expressing shDOT1L or shDCAF1.

(K and L) HIV-1 gag mRNA expression levels were detected upon TNFα (K) or prostratin (L) activation in $CD4^+$ HIV-1-infected cells. Data were normalized to shNC and are shown as means ± SD ($n = 4$).

(M) The model of a negative feedback loop for DOT1L to modulate HIV-1 reactivation. DOT1L in association with DCAF1 is recruited to HIV-1 LTR upon reactivation by NF-κB and mediates methylation at H3K79 sites, which may enhance DCAF1 occupancy at LTR. Recruited DCAF1 promotes ubiquitination of NF-κB and constrains its level at LTR and expression of HIV genes. Blocking DOT1L or DCAF1 in combination with LRA can promote HIV-1 reactivation. $^{***}p \leq 0.05$, $^{***}p \leq 0.001$. See also Figure S7 and Table S3.

efficacy of our method.[26,29] Moreover, our data reveal numerous proteins preferentially associated with H3K79me2 or H3K79me3, reminiscent of the differential genomic distribution of these two epigenetic marks and possibly distinct functions.[54–57] Many proteins associated with H3K79me2 belong to several complexes in transcriptional regulation. More interestingly, it has been shown that DOT1L is associated with RNAPII.[11,58] In other studies, a potential link between DOT1L and Tat was proposed as well.[59] It will be interesting in future studies to clarify how DOT1L is specifically recruited to the HIV locus and mediates transcriptional activity, together with H3K79me2 and other associated factors.

DCAF1 mediates the phosphorylation and ubiquitination of substrates involved in transcription.[37,38,46] It drives epigenetic silencing and oncogenic transformation by phosphorylating histone H2A at T120 and EZH2 at T367 in colon cancer.[46,60] In U2OS cells, MDM2 (murine double minute 2) interacts with DCAF1, the deletion of which drastically suppresses the MDM2-mediated p53 polyubiquitination and degradation.[37] Consistently, knockdown of DCAF1 leads to enhanced recruitment of p53 to chromatin in prostate cancer cells.[61] During HIV-1 infection, Vpr activates the host CRL4-DCAF1 E3 ligase to degrade the histone deacetylase SIRT7.[40] It also induces the degradation of two transcriptional regulators ZIP and sZIP by hijacking DCAF1.[62] Our findings here have revealed a negative feedback role of DCAF1 in repressing NF-κB-induced viral and non-viral genes at host genomic sites that are determined by DOT1L (Figure 7M), suggesting that the function of IκBα in clearing NF-κB from the nucleus may work in conjunction with DCAF1-mediated ubiquitination. These findings indicate the functional diversity of DCAF1 is determined by its association with various binding partners. Further investigation into the specific mechanism by which DCAF1 targets NF-κB for ubiquitination and clearance would be of great interest.

Feedback regulation is an important balancing mechanism for dynamic biological processes to maintain homeostasis in response to variable environmental conditions. A previous study has shown that at the transcriptional initiation stage, low levels of nascent RNAs tend to form condensates in cells, whereas high levels of RNA synthesis impede condensate formation and local transcription.[63] Interestingly, we previously discovered that an RNA-binding protein RBFox2 is recruited to near-gene promoters via nascent RNAs and represses transcription by mediating global PRC2 targeting.[64] Recently, it was reported that many transcription factors bind RNAs through previously unrecognized domains or peptide sequences.[65] Regarding the regulation of HIV-1 gene expression, it is worth mentioning DOT1L/DCAF1 axis functions not only for HIV-1 reactivation but also for the maintenance stage when TNFα stimulation is removed. Such observations indicate the feedback role mediated by DOT1L/DCAF1 may not be restricted to NF-κB, and other DCAF1 targets may exist as well, which wait for further investigation.

Administration of an LRA alone usually leads to unsatisfactory and inefficient reactivation of the HIV gene, due to variable responses to the reagent among individual patients and differences in cell or tissue types.[66–68] To tackle this issue, several studies have examined the combination of various LRA regulatory targets to trigger latent viral transcription in multiple cell types and compartments, followed by immunotherapy to maximize the clearance of the latent viral reservoir.[68,69] On the other hand, as the cellular response to HIV reactivation is not fully understood, a continuation of mechanistic studies aiming to identify new LRA targets is needed. EPZ5676 is a potent inhibitor of DOT1L, and its safety, tolerability, pharmacokinetics, pharmacodynamics, and anti-leukemia activity in relapsed/refractory adult leukemia patients have been extensively evaluated.[70] Therefore, the synergistic effect of EPZ5676 together with prostratin or JQ1 we observed in cell models warrants further evaluation of these combination recipes in more clinically relevant settings for HIV therapy.

More intriguingly, the main rationale behind the development of new LRAs for the "shock and kill" strategy is to promote the reactivation of the HIV genome, by either inducing gene expression with NF-κB pathway activators[49] or removing molecular hurdles that maintain the latency state, with HDAC inhibitors, JQ1, and SMAC mimetics.[71] From a new perspective, our work indicates that upon HIV reactivation, host cells may respond to initiate inherent regulatory mechanisms to antagonize such harmful viral activities. This finding provides an alternative explanation for the lack of effectiveness of current LRAs used as a single reagent. Moreover, we demonstrate here that by deactivating this host defense system, synergistic effects on HIV reactivation are expected when combined with known activators. By continuing to elucidate the molecular components of the negative feedback mechanisms during HIV reactivation, the new drug combination with the two-pronged approach may enable more comprehensive and efficient viral induction and clearance in the future.

Limitations of the study

Several limitations exist. The peptide pull-down assay for analyzing H3K79 methylated proteins was performed under a less natural condition than the nucleosome-based interaction assays; therefore, any candidate proteins in the association list of our proteomics data that are of interest for future studies need to be validated *in vivo*. Moreover, while we have identified that DCAF1 is associated with both DOT1L and H3K79me2, what exactly are the molecular basis and chain reactions for DOT1L to bind to DCAF1 and facilitate its recruitment to chromatin, where the H3K79 is methylated, remain elusive. Interestingly, although our data indicate that DCAF1 represses the HIV reactivation in response to TNFα through antagonizing NF-κB binding at LTR, it has a similar role in response to JQ1, which induces HIV reactivation independent of NF-κB signaling. Such an observation suggests an alternative regulatory mechanism by DCAF1 waits for further exploration. Lastly, we only tested the effect of DOT1L and DCAF1 in primary cells from two patients. It is known that HIV infection is linked to heterogeneous pathologies among patients, necessitating further validation with an expanded sample size of patients.

STAR★METHODS

Detailed methods are provided in the online version of this paper and include the following:

- KEY RESOURCES TABLE
- RESOURCE AVAILABILITY

SUPPLEMENTAL INFORMATION

Supplemental information can be found online at https://doi.org/10.1016/j.celrep.2024.114368.

ACKNOWLEDGMENTS

We would like to thank all the members who participated in this research. We thank Peixin Yuan from Wuhan University for instructing the use of a mass spectrometer and revising the method description. We also thank Dr. Liang Cheng and Fei Luo from Medical Research Institute at Wuhan University for project discussion and help in hypothesis testing as well as Shan Zhang and Benzhe Ji from Wuhan University for providing FLAG-p65 and NF-κB-luciferase plasmids. This work was supported by the National Natural Science Foundation of China (31970619 and 32171289), National Key Research and Development Program of China (2021YFA1100500), and the Fundamental Research Funds for the Central Universities (2042022rc0008).

AUTHOR CONTRIBUTIONS

Conceptualization: L.C. and F.L. Design of experiments: F.L., L.C., A.J., and D.H. Conducted experiments and analysis: F.L., J.J., J.D., X.C., and A.J. RNA-seq data and mass spectrometry analysis: Q.L., H.G., Y.Z., K.W., F.Y., and X.Z. Supervision: L.C. Writing—original draft: F.L. and L.C. Writing—review and editing: all authors.

DECLARATION OF INTERESTS

The authors declare no competing interests.

Received: January 3, 2024
Revised: May 6, 2024
Accepted: May 31, 2024

REFERENCES

1. Lee, J.M., Hammarén, H.M., Savitski, M.M., and Baek, S.H. (2023). Control of protein stability by post-translational modifications. Nat. Commun. *14*, 201. https://doi.org/10.1038/s41467-023-35795-8.
2. van Leeuwen, F., Gafken, P.R., and Gottschling, D.E. (2002). Dot1p modulates silencing in yeast by methylation of the nucleosome core. Cell *109*, 745–756. https://doi.org/10.1016/s0092-8674(02)00759-6.
3. Worden, E.J., Hoffmann, N.A., Hicks, C.W., and Wolberger, C. (2019). Mechanism of Cross-talk between H2B Ubiquitination and H3 Methylation by Dot1L. Cell *176*, 1490–1501.e12. https://doi.org/10.1016/j.cell.2019.02.002.
4. Anderson, C.J., Baird, M.R., Hsu, A., Barbour, E.H., Koyama, Y., Borgnia, M.J., and McGinty, R.K. (2019). Structural Basis for Recognition of Ubiquitylated Nucleosome by Dot1L Methyltransferase. Cell Rep. *26*, 1681–1690.e5. https://doi.org/10.1016/j.celrep.2019.01.058.
5. Jang, S., Kang, C., Yang, H.-S., Jung, T., Hebert, H., Chung, K.Y., Kim, S.J., Hohng, S., and Song, J.-J. (2019). Structural basis of recognition and destabilization of the histone H2B ubiquitinated nucleosome by the DOT1L histone H3 Lys79 methyltransferase. Genes Dev. *33*, 620–625. https://doi.org/10.1101/gad.323790.118.
6. Yao, T., Jing, W., Hu, Z., Tan, M., Cao, M., Wang, Q., Li, Y., Yuan, G., Lei, M., and Huang, J. (2019). Structural basis of the crosstalk between histone H2B monoubiquitination and H3 lysine 79 methylation on nucleosome. Cell Res. *29*, 330–333. https://doi.org/10.1038/s41422-019-0146-7.
7. Valencia-Sánchez, M.I., De Ioannes, P., Wang, M., Vasilyev, N., Chen, R., Nudler, E., Armache, J.-P., and Armache, K.-J. (2019). Structural Basis of Dot1L Stimulation by Histone H2B Lysine 120 Ubiquitination. Mol Cell *74*, 1010–1019.e6.. https://doi.org/10.1016/j.molcel.2019.03.029.
8. Okada, Y., Feng, Q., Lin, Y., Jiang, Q., Li, Y., Coffield, V.M., Su, L., Xu, G., and Zhang, Y. (2005). hDOT1L links histone methylation to leukemogenesis. Cell *121*, 167–178. https://doi.org/10.1016/j.cell.2005.02.020.
9. Cao, K., Ugarenko, M., Ozark, P.A., Wang, J., Marshall, S.A., Rendleman, E.J., Liang, K., Wang, L., Zou, L., Smith, E.R., et al. (2020). DOT1L-controlled cell-fate determination and transcription elongation are independent of H3K79 methylation. Proc. Natl. Acad. Sci. USA *117*, 27365–27373. https://doi.org/10.1073/pnas.2001075117.
10. Godfrey, L., Crump, N.T., Thorne, R., Lau, I.J., Repapi, E., Dimou, D., Smith, A.L., Harman, J.R., Telenius, J.M., Oudelaar, A.M., et al. (2019). DOT1L inhibition reveals a distinct subset of enhancers dependent on H3K79 methylation. Nat. Commun. *10*, 2803. https://doi.org/10.1038/s41467-019-10844-3.
11. Kim, S.-K., Jung, I., Lee, H., Kang, K., Kim, M., Jeong, K., Kwon, C.S., Han, Y.-M., Kim, Y.S., Kim, D., et al. (2012). Human histone H3K79 methyltransferase DOT1L protein [corrected] binds actively transcribing RNA polymerase II to regulate gene expression. J. Biol. Chem. *287*, 39698–39709. https://doi.org/10.1074/jbc.M112.384057.
12. Okuda, H., Stanojevic, B., Kanai, A., Kawamura, T., Takahashi, S., Matsui, H., Takaori-Kondo, A., and Yokoyama, A. (2017). Cooperative gene activation by AF4 and DOT1L drives MLL-rearranged leukemia. J. Clin. Invest. *127*, 1918–1931. https://doi.org/10.1172/JCI91406.
13. Olsen, S.N., Godfrey, L., Healy, J.P., Choi, Y.A., Kai, Y., Hatton, C., Perner, F., Haarer, E.L., Nabet, B., Yuan, G.-C., et al. (2022). MLL::AF9 degradation induces rapid changes in transcriptional elongation and subsequent loss of an active chromatin landscape. Mol. Cell *82*, 1140–1155.e11. https://doi.org/10.1016/j.molcel.2022.02.013.
14. Li, Y., Wen, H., Xi, Y., Tanaka, K., Wang, H., Peng, D., Ren, Y., Jin, Q., Dent, S.Y.R., Li, W., et al. (2014). AF9 YEATS domain links histone acetylation to DOT1L-mediated H3K79 methylation. Cell *159*, 558–571. https://doi.org/10.1016/j.cell.2014.09.049.
15. Vatapalli, R., Sagar, V., Rodriguez, Y., Zhao, J.C., Unno, K., Pamarthy, S., Lysy, B., Anker, J., Han, H., Yoo, Y.A., et al. (2020). Histone methyltransferase DOT1L coordinates AR and MYC stability in prostate cancer. Nat. Commun. *11*, 4153. https://doi.org/10.1038/s41467-020-18013-7.
16. Zhang, J., Yang, T., Han, M., Wang, X., Yang, W., Guo, N., Ren, Y., Cui, W., Li, S., Zhao, Y., et al. (2023). Gain-of-function mutations in the catalytic domain of DOT1L promote lung cancer malignant phenotypes via the MAPK/ERK signaling pathway. Sci. Adv. *9*, eadc9273. https://doi.org/10.1126/sciadv.adc9273.

17. Jones, B., Su, H., Bhat, A., Lei, H., Bajko, J., Hevi, S., Baltus, G.A., Kadam, S., Zhai, H., Valdez, R., et al. (2008). The histone H3K79 methyltransferase Dot1L is essential for mammalian development and heterochromatin structure. PLoS Genet. *4*, e1000190. https://doi.org/10.1371/journal.pgen.1000190.

18. Singer, M.S., Kahana, A., Wolf, A.J., Meisinger, L.L., Peterson, S.E., Goggin, C., Mahowald, M., and Gottschling, D.E. (1998). Identification of high-copy disruptors of telomeric silencing in Saccharomyces cerevisiae. Genetics *150*, 613–632. https://doi.org/10.1093/genetics/150.2.613.

19. Ng, H.H., Feng, Q., Wang, H., Erdjument-Bromage, H., Tempst, P., Zhang, Y., and Struhl, K. (2002). Lysine methylation within the globular domain of histone H3 by Dot1 is important for telomeric silencing and Sir protein association. Genes Dev. *16*, 1518–1527. https://doi.org/10.1101/gad.1001502.

20. Malla, A.B., Yu, H., Farris, D., Kadimi, S., Lam, T.T., Cox, A.L., Smith, Z.D., and Lesch, B.J. (2023). DOT1L bridges transcription and heterochromatin formation at mammalian pericentromeres. EMBO Rep. *24*, e56492. https://doi.org/10.15252/embr.202256492.

21. Zhao, X., Li, X., Sun, H., Zhao, X., Gao, T., Shi, P., Chen, F., Liu, L., and Lu, X. (2023). Dot1l cooperates with Npm1 to repress endogenous retrovirus MERVL in embryonic stem cells. Nucleic Acids Res. *51*, 8970–8986. https://doi.org/10.1093/nar/gkad640.

22. Wan, S., Zhou, Y., Huang, Q., and Yang, Y. (2021). Dot1l Aggravates Keratitis Induced by Herpes Simplex Virus Type 1 in Mice via p38 MAPK-Mediated Oxidative Stress. Oxid. Med. Cell. Longev. *2021*, 6612689. https://doi.org/10.1155/2021/6612689.

23. Marcos-Villar, L., Díaz-Colunga, J., Sandoval, J., Zamarreño, N., Landeras-Bueno, S., Esteller, M., Falcón, A., and Nieto, A. (2018). Epigenetic control of influenza virus: role of H3K79 methylation in interferon-induced antiviral response. Sci. Rep. *8*, 1230. https://doi.org/10.1038/s41598-018-19370-6.

24. Marcos-Villar, L., and Nieto, A. (2019). The DOT1L inhibitor Pinometostat decreases the host-response against infections: Considerations about its use in human therapy. Sci. Rep. *9*, 16862. https://doi.org/10.1038/s41598-019-53239-6.

25. Chen, S., Wang, D., Liu, Y., Zhao, R., Wu, T., Hu, X., Pan, Z., and Cui, H. (2020). Targeting the Histone Methyltransferase Disruptor of Telomeric Silencing 1-Like Restricts Avian Leukosis Virus Subgroup J Replication by Restoring the Innate Immune Response in Chicken Macrophages. Front. Microbiol. *11*, 603131. https://doi.org/10.3389/fmicb.2020.603131.

26. Lin, J., Wu, Y., Tian, G., Yu, D., Yang, E., Lam, W.H., Liu, Z., Jing, Y., Dang, S., Bao, X., et al. (2023). Menin "reads" H3K79me2 mark in a nucleosomal context. Science *379*, 717–723. https://doi.org/10.1126/science.adc9318.

27. Huyen, Y., Zgheib, O., Ditullio, R.A., Gorgoulis, V.G., Zacharatos, P., Petty, T.J., Sheston, E.A., Mellert, H.S., Stavridi, E.S., and Halazonetis, T.D. (2004). Methylated lysine 79 of histone H3 targets 53BP1 to DNA double-strand breaks. Nature *432*, 406–411. https://doi.org/10.1038/nature03114.

28. Sabra, M., Texier, P., El Maalouf, J., and Lomonte, P. (2013). The Tudor protein survival motor neuron (SMN) is a chromatin-binding protein that interacts with methylated lysine 79 of histone H3. J. Cell Sci. *126*, 3664–3677. https://doi.org/10.1242/jcs.126003.

29. Kang, J.-Y., Kim, J.-Y., Kim, K.-B., Park, J.W., Cho, H., Hahm, J.Y., Chae, Y.-C., Kim, D., Kook, H., Rhee, S., et al. (2018). KDM2B is a histone H3K79 demethylase and induces transcriptional repression via sirtuin-1-mediated chromatin silencing. FASEB J *32*, 5737–5750. https://doi.org/10.1096/fj.201800242R.

30. Fischle, W. (2012). One, two, three: how histone methylation is read. Epigenomics *4*, 641–653. https://doi.org/10.2217/epi.12.56.

31. Lee, J.M., Lee, J.S., Kim, H., Kim, K., Park, H., Kim, J.-Y., Lee, S.H., Kim, I.S., Kim, J., Lee, M., et al. (2012). EZH2 generates a methyl degron that is recognized by the DCAF1/DDB1/CUL4 E3 ubiquitin ligase complex. Mol. Cell *48*, 572–586. https://doi.org/10.1016/j.molcel.2012.09.004.

32. Lu, X., Zhu, X., Li, Y., Liu, M., Yu, B., Wang, Y., Rao, M., Yang, H., Zhou, K., Wang, Y., et al. (2016). Multiple P-TEFbs cooperatively regulate the release of promoter-proximally paused RNA polymerase II. Nucleic Acids Res. *44*, 6853–6867. https://doi.org/10.1093/nar/gkw571.

33. Hagkarim, N.C., Hajkarim, M.C., Suzuki, T., Fujiwara, T., Winkler, G.S., Stewart, G.S., and Grand, R.J. (2023). Disruption of the Mammalian Ccr4-Not Complex Contributes to Transcription-Mediated Genome Instability. Cells *12*, 1868. https://doi.org/10.3390/cells12141868.

34. Park, I.-G., Jeon, M., Kim, H., and Lee, J.M. (2022). Coordinated methyl readers: Functional communications in cancer. Semin. Cancer Biol. *83*, 88–99. https://doi.org/10.1016/j.semcancer.2021.03.015.

35. Maurer-Stroh, S., Dickens, N.J., Hughes-Davies, L., Kouzarides, T., Eisenhaber, F., and Ponting, C.P. (2003). The Tudor domain 'Royal Family': Tudor, plant Agenet, Chromo, PWWP and MBT domains. Trends Biochem. Sci. *28*, 69–74.

36. Zhou, X., DeLucia, M., Hao, C., Hrecka, K., Monnie, C., Skowronski, J., and Ahn, J. (2017). HIV-1 Vpr protein directly loads helicase-like transcription factor (HLTF) onto the CRL4-DCAF1 E3 ubiquitin ligase. J. Biol. Chem. *292*, 21117–21127. https://doi.org/10.1074/jbc.M117.798801.

37. Guo, Z., Kong, Q., Liu, C., Zhang, S., Zou, L., Yan, F., Whitmire, J.K., Xiong, Y., Chen, X., and Wan, Y.Y. (2016). DCAF1 controls T-cell function via p53-dependent and -independent mechanisms. Nat. Commun. *7*, 10307. https://doi.org/10.1038/ncomms10307.

38. Hrecka, K., Gierszewska, M., Srivastava, S., Kozaczkiewicz, L., Swanson, S.K., Florens, L., Washburn, M.P., and Skowronski, J. (2007). Lentiviral Vpr usurps Cul4-DDB1[VprBP] E3 ubiquitin ligase to modulate cell cycle. Proc. Natl. Acad. Sci. USA *104*, 11778–11783.

39. He, N., Chan, C.K., Sobhian, B., Chou, S., Xue, Y., Liu, M., Alber, T., Benkirane, M., and Zhou, Q. (2011). Human Polymerase-Associated Factor complex (PAFc) connects the Super Elongation Complex (SEC) to RNA polymerase II on chromatin. Proc. Natl. Acad. Sci. USA *108*, E636–E645. https://doi.org/10.1073/pnas.1107107108.

40. Zhou, X., Monnie, C., DeLucia, M., and Ahn, J. (2021). HIV-1 Vpr activates host CRL4-DCAF1 E3 ligase to degrade histone deacetylase SIRT7. Virol. J. *18*, 48. https://doi.org/10.1186/s12985-021-01514-2.

41. Pearson, R., Kim, Y.K., Hokello, J., Lassen, K., Friedman, J., Tyagi, M., and Karn, J. (2008). Epigenetic silencing of human immunodeficiency virus (HIV) transcription by formation of restrictive chromatin structures at the viral long terminal repeat drives the progressive entry of HIV into latency. J. Virol. *82*, 12291–12303. https://doi.org/10.1128/JVI.01383-08.

42. Gao, R., Bao, J., Yan, H., Xie, L., Qin, W., Ning, H., Huang, S., Cheng, J., Zhi, R., Li, Z., et al. (2020). Competition between PAF1 and MLL1/COMPASS confers the opposing function of LEDGF/p75 in HIV latency and proviral reactivation. Sci. Adv. *6*, eaaz8411. https://doi.org/10.1126/sciadv.aaz8411.

43. Arenzana-Seisdedos, F., Thompson, J., Rodriguez, M.S., Bachelerie, F., Thomas, D., and Hay, R.T. (1995). Inducible nuclear expression of newly synthesized I kappa B alpha negatively regulates DNA-binding and transcriptional activities of NF-kappa B. Mol. Cell Biol. *15*, 2689–2696. https://doi.org/10.1128/MCB.15.5.2689.

44. Tran, K., Merika, M., and Thanos, D. (1997). Distinct functional properties of IkappaB alpha and IkappaB beta. Mol. Cell Biol. *17*, 5386–5399. https://doi.org/10.1128/MCB.17.9.5386.

45. Wille, C.K., and Sridharan, R. (2022). Connecting the DOTs on Cell Identity. Front. Cell Dev. Biol. *10*, 906713. https://doi.org/10.3389/fcell.2022.906713.

46. Kim, K., Kim, J.-M., Kim, J.-S., Choi, J., Lee, Y.S., Neamati, N., Song, J.S., Heo, K., and An, W. (2013). VprBP has intrinsic kinase activity targeting histone H2A and represses gene transcription. Mol. Cell *52*, 459–467. https://doi.org/10.1016/j.molcel.2013.09.017.

47. Huang, F., Yao, W., Sun, B., and Fujinaga, K. (2022). DCAF1 inhibits the NF-κB pathway by targeting p65. Immunol. Lett. *249*, 33–42. https://doi.org/10.1016/j.imlet.2022.08.005.

48. Wang, H., Liu, Y., Huan, C., Yang, J., Li, Z., Zheng, B., Wang, Y., and Zhang, W. (2020). NF-κB-Interacting Long Noncoding RNA Regulates HIV-1 Replication and Latency by Repressing NF-κB Signaling. J. Virol. *94*, e01057-20. https://doi.org/10.1128/JVI.01057-20.

49. Kim, Y., Anderson, J.L., and Lewin, S.R. (2018). Getting the "Kill" into "Shock and Kill": Strategies to Eliminate Latent HIV. Cell Host Microbe *23*, 14–26. https://doi.org/10.1016/j.chom.2017.12.004.

50. Nühn, M.M., Gumbs, S.B.H., Buchholtz, N.V.E.J., Jannink, L.M., Gharu, L., de Witte, L.D., Wensing, A.M.J., Lewin, S.R., Nijhuis, M., and Symons, J. (2022). Shock and kill within the CNS: A promising HIV eradication approach? J. Leukoc. Biol. *112*, 1297–1315. https://doi.org/10.1002/JLB.5VMR0122-046RRR.

51. Cao, S., and Woodrow, K.A. (2019). Nanotechnology approaches to eradicating HIV reservoirs. Eur. J. Pharm. Biopharm. *138*, 48–63. https://doi.org/10.1016/j.ejpb.2018.06.002.

52. Kulkosky, J., Culnan, D.M., Roman, J., Dornadula, G., Schnell, M., Boyd, M.R., and Pomerantz, R.J. (2001). Prostratin: activation of latent HIV-1 expression suggests a potential inductive adjuvant therapy for HAART. Blood *98*, 3006–3015. https://doi.org/10.1182/blood.v98.10.3006.

53. Conrad, R.J., Fozouni, P., Thomas, S., Sy, H., Zhang, Q., Zhou, M.-M., and Ott, M. (2017). The Short Isoform of BRD4 Promotes HIV-1 Latency by Engaging Repressive SWI/SNF Chromatin-Remodeling Complexes. Mol. Cell *67*, 1001–1012.e6. https://doi.org/10.1016/j.molcel.2017.07.025.

54. Barski, A., Cuddapah, S., Cui, K., Roh, T.-Y., Schones, D.E., Wang, Z., Wei, G., Chepelev, I., and Zhao, K. (2007). High-resolution profiling of histone methylations in the human genome. Cell *129*, 823–837. https://doi.org/10.1016/j.cell.2007.05.009.

55. Black, J.C., Van Rechem, C., and Whetstine, J.R. (2012). Histone lysine methylation dynamics: establishment, regulation, and biological impact. Mol. Cell *48*, 491–507. https://doi.org/10.1016/j.molcel.2012.11.006.

56. Ernst, J., Kheradpour, P., Mikkelsen, T.S., Shoresh, N., Ward, L.D., Epstein, C.B., Zhang, X., Wang, L., Issner, R., Coyne, M., et al. (2011). Mapping and analysis of chromatin state dynamics in nine human cell types. Nature *473*, 43–49. https://doi.org/10.1038/nature09906.

57. Liu, T., Rechtsteiner, A., Egelhofer, T.A., Vielle, A., Latorre, I., Cheung, M.-S., Ercan, S., Ikegami, K., Jensen, M., Kolasinska-Zwierz, P., et al. (2011). Broad chromosomal domains of histone modification patterns in C. elegans. Genome Res. *21*, 227–236. https://doi.org/10.1101/gr.115519.110.

58. Wu, A., Zhi, J., Tian, T., Cihan, A., Cevher, M.A., Liu, Z., David, Y., Muir, T.W., Roeder, R.G., and Yu, M. (2021). DOT1L complex regulates transcriptional initiation in human erythroleukemic cells. Proc. Natl. Acad. Sci. USA *118*, e2106148118. https://doi.org/10.1073/pnas.2106148118.

59. Reeder, J.E., Kwak, Y.-T., McNamara, R.P., Forst, C.V., and D'Orso, I. (2015). HIV Tat controls RNA Polymerase II and the epigenetic landscape to transcriptionally reprogram target immune cells. Elife *4*, e08955. https://doi.org/10.7554/eLife.08955.

60. Ghate, N.B., Kim, S., Shin, Y., Kim, J., Doche, M., Valena, S., Situ, A., Kim, S., Rhie, S.K., Lenz, H.-J., et al. (2023). Phosphorylation and stabilization of EZH2 by DCAF1/VprBP trigger aberrant gene silencing in colon cancer. Nat. Commun. *14*, 2140. https://doi.org/10.1038/s41467-023-37883-1.

61. Poulose, N., Forsythe, N., Polonski, A., Gregg, G., Maguire, S., Fuchs, M., Minner, S., Sauter, G., McDade, S.S., and Mills, I.G. (2022). VPRBP Functions Downstream of the Androgen Receptor and OGT to Restrict p53 Activation in Prostate Cancer. Mol. Cancer Res. *20*, 1047–1060. https://doi.org/10.1158/1541-7786.MCR-21-0477.

62. Maudet, C., Sourisce, A., Dragin, L., Lahouassa, H., Rain, J.-C., Bouaziz, S., Ramirez, B.C., and Margottin-Goguet, F. (2013). HIV-1 Vpr induces the degradation of ZIP and sZIP, adaptors of the NuRD chromatin remodeling complex, by hijacking DCAF1/VprBP. PLoS One *8*, e77320. https://doi.org/10.1371/journal.pone.0077320.

63. Henninger, J.E., Oksuz, O., Shrinivas, K., Sagi, I., LeRoy, G., Zheng, M.M., Andrews, J.O., Zamudio, A.V., Lazaris, C., Hannett, N.M., et al. (2021). RNA-Mediated Feedback Control of Transcriptional Condensates. Cell *184*, 207–225.e24. https://doi.org/10.1016/j.cell.2020.11.030.

64. Wei, C., Xiao, R., Chen, L., Cui, H., Zhou, Y., Xue, Y., Hu, J., Zhou, B., Tsutsui, T., Qiu, J., et al. (2016). RBFox2 Binds Nascent RNA to Globally Regulate Polycomb Complex 2 Targeting in Mammalian Genomes. Mol. Cell *62*, 875–889. https://doi.org/10.1016/j.molcel.2016.04.013.

65. Oksuz, O., Henninger, J.E., Warneford-Thomson, R., Zheng, M.M., Erb, H., Vancura, A., Overholt, K.J., Hawken, S.W., Banani, S.F., Lauman, R., et al. (2023). Transcription factors interact with RNA to regulate genes. Mol. Cell *83*, 2449–2463.e13. https://doi.org/10.1016/j.molcel.2023.06.012.

66. Pardons, M., Fromentin, R., Pagliuzza, A., Routy, J.-P., and Chomont, N. (2019). Latency-Reversing Agents Induce Differential Responses in Distinct Memory CD4 T Cell Subsets in Individuals on Antiretroviral Therapy. Cell Rep. *29*, 2783–2795.e5. https://doi.org/10.1016/j.celrep.2019.10.101.

67. Grau-Expósito, J., Luque-Ballesteros, L., Navarro, J., Curran, A., Burgos, J., Ribera, E., Torrella, A., Planas, B., Badía, R., Martin-Castillo, M., et al. (2019). Latency reversal agents affect differently the latent reservoir present in distinct CD4+ T subpopulations. PLoS Pathog. *15*, e1007991. https://doi.org/10.1371/journal.ppat.1007991.

68. Bullen, C.K., Laird, G.M., Durand, C.M., Siliciano, J.D., and Siliciano, R.F. (2014). New ex vivo approaches distinguish effective and ineffective single agents for reversing HIV-1 latency in vivo. Nat. Med. *20*, 425–429. https://doi.org/10.1038/nm.3489.

69. Spivak, A.M., and Planelles, V. (2018). Novel Latency Reversal Agents for HIV-1 Cure. Annu. Rev. Med. *69*, 421–436. https://doi.org/10.1146/annurev-med-052716-031710.

70. Stein, E.M., Garcia-Manero, G., Rizzieri, D.A., Tibes, R., Berdeja, J.G., Savona, M.R., Jongen-Lavrenic, M., Altman, J.K., Thomson, B., Blakemore, S.J., et al. (2018). The DOT1L inhibitor pinometostat reduces H3K79 methylation and has modest clinical activity in adult acute leukemia. Blood *131*, 2661–2669. https://doi.org/10.1182/blood-2017-12-818948.

71. Pache, L., Dutra, M.S., Spivak, A.M., Marlett, J.M., Murry, J.P., Hwang, Y., Maestre, A.M., Manganaro, L., Vamos, M., Teriete, P., et al. (2015). BIRC2/cIAP1 Is a Negative Regulator of HIV-1 Transcription and Can Be Targeted by Smac Mimetics to Promote Reversal of Viral Latency. Cell Host Microbe *18*, 345–353. https://doi.org/10.1016/j.chom.2015.08.009.

72. Barger, C.J., Branick, C., Chee, L., and Karpf, A.R. (2019). Pan-Cancer Analyses Reveal Genomic Features of FOXM1 Overexpression in Cancer. Cancers *11*, 251. https://doi.org/10.3390/cancers11020251.

73. Van Nostrand, E.L., Freese, P., Pratt, G.A., Wang, X., Wei, X., Xiao, R., Blue, S.M., Chen, J.-Y., Cody, N.A.L., Dominguez, D., et al. (2020). A large-scale binding and functional map of human RNA-binding proteins. Nature *583*, 711–719. https://doi.org/10.1038/s41586-020-2077-3.

STAR★METHODS

KEY RESOURCES TABLE

REAGENT or RESOURCE	SOURCE	IDENTIFIER
Antibodies		
NELFE	Proteintech	Cat#10705-1-AP; RRID:AB_513966
CPSF6	abclonal	Cat#A5963; RRID:AB_2766688
CPSF3L	abclonal	Cat#A6566; RRID:AB_2767160
CBX8	abclonal	Cat#A6222; RRID:AB_2766831
DCAF1	Proteintech	Cat#11612-1-AP; RRID:AB_2216933
MED23	abclonal	Cat#A10163; RRID:AB_2757691
INTS9	abclonal	Cat#A4847; RRID:AB_2765902
Nucleolin	Proteintech	Cat#10556-1-AP; RRID:AB_2082423
H3	abclonal	Cat#A2348; RRID:AB_2631273
H3	abcam	Cat #ab1791 RRID: AB_302613
Men1	Proteintech	Cat#15159-1-AP; RRID:AB_2250607
LamB1	Proteintech	Cat#67705-1-Ig; RRID:AB_2882896
GFP	abclonal	Cat#AE012; RRID:AB_2770402
actin	abclonal	Cat#A2319; RRID:AB_2862994
GAPDH	abclonal	Cat#AC035; RRID:AB_2769863
Tubulin	abclonal	Cat#AC012; RRID:AB_2768341
DOT1L (D1W4Z)	CST	Cat#77087S; RRID:AB_2799889
DOT1L	abcam	Cat#ab72454; RRID:AB_1269271
H3K79me2	abcam	Cat#ab3594; RRID:AB_303937
Rpb1 NTD (D8L4Y)	CST	Cat#14958S; RRID:AB_2687876
DDB1	abcam	Cat#ab109027; RRID:AB_10859111
NF-κB p65 (D14E12) XP Rabbit mAb	CST	Cat#8242; RRID:AB_10859369
CHD8	Proteintech	Cat#29783-1-AP; RRID:AB_2918347
HA	Millipore Sigma	Cat#H3663; RRID:AB_262051
Flag	sigma	Cat#F1804; RRID:AB_262044
myc(9E10)	Santa Cruz	Cat#sc-40; RRID:AB_627268
Anti-Ubiquitin (linkage-specific K48)	Abcam	Cat# ab140601; RRID:AB_2783797
HRP-conjugated Goat Anti-Rabbit IgG Heavy Chain	abclonal	Cat#AS063; RRID:AB_2864057
HRP-conjugated Goat Anti-Mouse IgG Heavy Chain	abclonal	Cat#AS064; RRID:AB_2864058
HRP-conjugated Goat Anti-Mouse IgG Light Chain	abclonal	Cat#A25012; RRID:AB_2737290
HRP Goat Anti-Rabbit IgG (H + L)	abclonal	Cat#AS014; RRID:AB_2769854
HRP Goat Anti-Mouse IgG (H + L)	abclonal	Cat#AS003; RRID:AB_2769851
Alexa Fluor 488 Goat anti-rabbit	Invitrogen	Cat#A-11008; RRID:AB_143165
Alexa Fluor 594 Goat anti-mouse	Invitrogen	Cat#A-11005; RRID:AB_2534073
Alexa Fluor 594 Goat anti-rabbit	Invitrogen	Cat#A-11012; RRID:AB_2534079
Chemicals, peptides, and recombinant proteins		
TNFα	Peprotech	300-01A
JQ1	selleck	S7110
Prostratin	Sigma-Aldrich	60857-08-1
Pinometostat (EPZ5676)	selleck	S7062
Doxycycline hyclate	Yeasen	CAS 24390-14-5
Formic acid	Thermo Fisher Scientific	A117-50
DTT	Thermo Fisher Pierce	20291

(*Continued on next page*)

Continued

REAGENT or RESOURCE	SOURCE	IDENTIFIER
Iodoacetamide (IAA)	Sigma-Aldrich	I1149-5G
Acetonitrile(ACN)	Thermo Fisher Scientific	A9554
Trypsin	Promega	V5111
Critical commercial assays		
Dual-Luciferase® Reporter Assay System	Promega	E1910;
TRIzol™	Invitrogen™	15596026
High purity plasmid small extract medium dose kit	TianGen	DP107
Q5 mutagenesis kit	NEB	Cat #E0552S
2X MultiF Seamless Assembly Mix	Abclonal	RK21020
Deposited data		
Mass spectrometry enriched protein list	This manuscript	Table S1
Mass spectrometry data	This manuscript	OMIX006500
RNA-seq	This manuscript	GSA-Human: HRA005975
Experimental models: Cell lines		
HEK293T, Human, Epithelial Kidney Cells	ATCC	CRL-3216, RRID: CVCL_0063
Jurkat E4, derived from Jurkat cells	Ru et al., Pearson et al.[41,42]	N/A
Jurkat 2D10, derived from Jurkat cells	Ru et al., Pearson et al.[41,42]	N/A
Primary CD4+ T cells	Milestone® Biotechnologies	N/A
Experimental models: Organisms/strains		
Trans10 Chemically Competent Cell	TransGen Biotech	CD101-01
Trans5α Chemically Competent Cell	TransGen Biotech	CD201-01
TransStbl3 Chemically Competent Cell	TransGen Biotech	CD521-01
Oligonucleotides		
1#siDCAF1-F	GenePharma	GCGACUCAUUCUCCAAUAUTT
1#siDCAF1-R	GenePharma	AUAUUGGAGAAUGAGUCGCTT
2#siDCAF1-F	GenePharma	GGAGGGAAUUGUCGAGAAUTT
2#siDCAF1-R	GenePharma	AUUCUCGACAAUUCCCUCCTT
1#siDOT1L-1 F	GenePharma	GCUGCCGGUCUACGAUAAATT
1#siDOT1L-1 R	GenePharma	UUUAUCGUAGACCGGCAGCTT
2#siDot1l –2 F	GenePharma	CGCCAACACGAGTGTTATATTTT
2#iDot1l –2 R	GenePharma	AATATAACACTCGTGTTGGCG
siNC-F	GenePharma	UUCUCCGAACGUGUCACGU
siNC-R	GenePharma	ACGUGACACGUUCGGAGAA
shDOT1L-1	TRCN0000020209	CCGGCGCCAACACGAGTGTTATA TTCTCGAGAATATAACACTCG TGTTGGCGTTTTTG
shDOT1L-2	This manuscript	CCGGCGAGTGTTATATTTGTGA ATACTCGAGTATTCACAAATAT AACACTCGTTTTTG
shDCAF1-1	TRCN0000129909	CCGGGCTGAGAATACTCTTCAA GAACTCGAGTTCTTGAAGAGT ATTCTCAGCTTTTTG
shDCAF1-1	TRCN0000129579	CCGGCCTCCCATTCTTCTGCC TTTACTCGAGTAAAGGCAGA AGAATGGGAGGTTTTTG
shDCAF1-2	This manuscript	CCGGCGAGAAACTGAGTCAAA TGAACTCGAGTTCATTTGACTC AGTTTCTCGTTTTTG

(*Continued on next page*)

Continued		
REAGENT or RESOURCE	SOURCE	IDENTIFIER
shNC	This manuscript	CCGGCAACAAGATGAAGAGCA CCAACTCGAGTTGGTGCTCTT CATCTTGTTGTTTTTG
Clone and ChIP-qPCR primers	Table S3	N/A
qRT-PCR primers	Table S3	N/A
Recombinant DNA		
Tet-on-plko.1	addgene	RRID:Addgene_21915
pCW57-MCS1-2A-MCS2	Adam Karpf[72]	RRID:Addgene_71782
pLVX-shRNA-Puro	OLIGOBIO Company	N/A
pCMV-myc	Youbio Company	N/A
ubiquitin mutant plasmids	Youbao Company	N/A
Software and algorithms		
Flowjo- V10	BD Biosciences	https://flowjo.bectondickinson.cn
Graphpad prism 8	Graphpad	https://www.graphpad-prism.cn/
ImageJ	National Institutes of Health (NIH)	https://imagej.net/software/imagej/

RESOURCE AVAILABILITY

Lead contact

Further information and requests for resources and reagents should be directed to and will be fulfilled by the lead contact, Liang Chen (liang_chen@whu.edu.cn).

Materials availability

All unique/stable reagents generated in this study are available from the lead contact with a completed Materials Transfer Agreement.

Data and code availability

- RNAseq data have been deposited at Gene Expression Omnibus (GEO): GSE (GSA-Human: HRA005975). Mass spectrometry proteomic data also have been deposited in the Open Archive for Miscellaneous Data (OMIX: OMIX006500) with https://ngdc.cncb.ac.cn/omix/.
- This paper does not report original code.
- Any additional information required to reanalyze the data reported in this work is available from the lead contact upon request

EXPERIMENTAL MODEL AND STUDY PARTICIPANT DETAILS

Cell lines

Jurkat E4 and 2D10 cells were cultured in RPMI 1640 (Gibco, C11875500BT) with 10% fetal bovine serum (FBS) (Gibco, 10110154) and 1% penicillin/streptomycin (Gibco, 15140-122) in a 37 °C incubator containing 5% CO_2. HEK293T cells were cultured in DMEM (Gibco, C11995500BT), supplemented with 10% fetal calf serum (ExCell Bio, FSP500) and 1% penicillin/streptomycin (Gibco) in a 37 °C incubator containing 5% CO_2. The E4 and 2D10 cells were gifts from Dr. Deqing Hu and Dr. Jonathan Karn. Two healthy donors provided the $CD4^+$ T cells, which were obtained from the Milestone Biological Science & Technology Co., Ltd. Primate $CD4^+$ T cells were cultured in RPMI 1640, which was enhanced with 1% penicillin/streptomycin, 10% FBS, 2.0 mM L-glutamine, and IL-2 (100 U/ml, Sino Biological, GMP-11848-HNAE).

METHOD DETAILS

Plasmid construction and screening of stable cell lines

The pRenilla-luciferase, pcDNA-Tat, and HIV-1 LTR-luciferase exressing vectors were gifts from Dr Deqing Hu. The Tet-on-pLKO.1 shRNA-expressing lentiviral vector was purchased from Sigma-Aldrich, and the one containing a scrambled shRNA was used as the control in this study. ShDOT1L-1 (TRCN0000020209), shDOT1L-2 (5′-3′ CGAGTGTTATATTTGTGAATA), shDCAF1-1 (TRCN0000129909; TRCN0000129579), shDCAF1-2 (5′-3′ CGAGAAACTGAGTCAAATGAA). pCW57-MCS1-2A-MCS2 was a gift from Adam Karpf (Addgene plasmid # 71782; http://n2t.net/addgene:71782; RRID:Addgene_71782).[72] Specifically, for preparation of the shRNA containing lentivirus and infection, the Tet-on-pLKO.1 vector was co-transfected with psPAX2 and pMD2G vectors into HEK293T cells. Supernatants were collected at 48 and 72 h after transfection and filtered through a 0.45 μm filter. To generate stable

cell lines, target cells were infected with freshly generated supernatants containing virus particles with specific shRNAs or empty vectors. Polybrene (10 μg/ml) was added during the infection. Two days later, cells were selected with puromycin (2 μg/mL; Sigma) for 14 days and positive clones were tested by Western blotting. The antibody and reagents are listed in Table S3. Cell lines stably expressing HA-DOT1L and HA-DCAF1 were constructed following similar viral preparation and infection protocols, using the pCW-HA-DOT1L or pCW-HA-DOT1L viral vectors. Primers used for plasmid construction are shown in Table S3.

RNA interference

DOT1L and DCAF1 siRNAs were purchased from GenePharma (Shanghai, China). Control siNC and target gene sequences are shown in Table S3. Lipofectamine RNAiMAX Transfection Reagent (Invitrogen, Carlsbad, CA, USA) was used to transfect siRNAs into HEK293T cells according to the manufacturer's instructions. For instance, We first transfected HEK293T cells with 10 pmol siDOT1L-1 or 10 pmol siDOT1L-2 in one well of a 24-well plate for 12 h. Next, the medium was replaced with fresh medium. Cells were harvested 48h after transfection for further assays. Primer sequences are listed in the Key resources table.

Cell viability assays

Cell viability was monitored using the CCK-8 Cell Counting Kit (A311, Vazyme Biotech Co., Ltd) following the manufacturer's instructions. In brief, Jurkat cells treated with DOX, EPZ5676, or TNFα were seeded in 96-well plates in RPMI-1640 medium containing 10% FBS at an equal density of 2×10^4 cells/well. Subsequently, 10 μL of CCK8 reagent was added to each well and incubated at 37°C for 2 h. Slightly different, the HEK293T cells need to be seeded in a 96-well plate at a density of 1×10^4 cells and cultured for 24 h. The following day, 100 μL of fresh DMEM medium should be replaced, followed by the addition of 10 μL of CCK8. Finally, absorbance was measured at 450 nm using a Microporous Plate Detecting Instrument (Cytation3, BioTek).

Mass spectrometry sample preparation

The LC–MS/MS analysis was conducted using the Mass spectrometry platform at Wuhan University. HEK293T cells were subjected to nuclear and cytoplasmic separation. The nucleus was then lysed and the resulting supernatant was collected. Dynabead MyOne Streptavidin C1 beads (65002, Invitrogen) were mixed with the supernatant for incubation at 4°C for 2 h to eliminate background noise and recover the supernatant. Meanwhile, freshly washed C1 beads were mixed with peptides with different numbers of methyl groups and incubated at 4°C for 4 h. The beads were subsequently washed, mixed with the nucleoplasm supernatant and incubated overnight at 4°C on a rotator. A portion of beads were eluted with SDS-PAGE loading buffer and subjected to silver staining for checking the eluted proteins. The rest of the beads were eluted for mass spectrometry experiments. The eluted protein samples were loaded onto the SDS-PAGE gel, after the bromophenol blue sample moved into the separation gel, the electrophoresis was stopped after 5 to 10 min, or until the bromophenol blue had moved 0.5 cm into the gel. Sliced the unstained SDS-PAGE gel into 1 mm^3 cubes and then digested by in-gel trypic digestion strategy. The gel pieces were reduced by 10 mM DTT at 56°C for 60 min and then alkylated with 55 mM iodoacetamide at room temperature for 45 min in the dark. The mixture was supplemented with trypsin at a final concentration of 5 ng/μL and incubated overnight at 37°C. Peptides were extracted from the gel pieces and desalted in a house-made stage-tip then dried using a speedvac to complete dryness.

Nano LC-MS/MS analysis

Nano-liquid chromatography tandem mass spectrometry (Nano-LC/MS/MS) was performed on a Thermo Scientific Q Exactive HF Orbitrap mass spectrometer. Peptides were separated on a C18-reversed phase column (25 cm long, 75 μm inner diameter) packed in-house with ReproSil-Pur C18-AQ resin. The HPLC gradient was as follows: 2–5% Solvent B (0.1% formic acid in acetonitrile) over 3 min, 5–35% B over 40 min, 35–44% B over 5 min, 44–90% B over 2 min, 90% B for 10 min at a flow-rate of 200 nL/min. Acquisition was performed in data-dependent acquisition (DDA) mode, and full MS scans with 1-micro scans at a 60,000 resolution were used over a mass range of m/z 350–1600 with detection in the Orbitrap. Automatic gain control (AGC) was set to 1×10^6, with dynamic exclusion (25 s) and charge state filtering enabled to remove unqualified singly charged peptides. After each scan, the 25 most abundant precursor ions were sequentially selected for HCD (Higher Energy Collision Induced Dissociation) fragmentation and MS/MS acquisition at 15,000 resolutions. HCD normalized collision energy (NCE) was set at 28%.

Mass spectrometry database searching

The raw data were processed and searched against the UniProt protein database (Homo sapiens) using Proteome Discoverer 2.1 (Thermo Scientific) software. Trypsin was chosen as specific enzyme, with two maximum missed cleavages allowed. The mass tolerance was 10 ppm and the MS/MS mass tolerance was 0.02Da. Peptides were filtered by 1% false discovery rate (FDR). Proteins were identified with at least 1 unique peptide with 1% FDR.

Mass spectrometry ternary graph analysis

The ternary graph was plotted according to Table S1 to show the distribution of specific recognition proteins of short peptides modified by different methylations of H3K79 (the colored dots indicated obvious enrichment, enrichment ratio ≥ 3, p value ≤ 0.05).

Specifically, the amount of each protein for each sample in triplicate was converted to a log2 value. The average value obtained from three sample repeats for a short peptide was compared to that for Random22, namely, the fold Change_log2. If the fold

Change_log2 value for a protein with a short peptide was greater than or equal to 3 and the *p*-value is less than or equal to 0.05, we consider that this protein is significantly associated with that peptide.

After screening significantly associated proteins for each peptide, the comparison between modified peptides will be conducted. If the relative fold Change_log2 value of a protein with one modified peptide (for example, peptide A) is three times larger than the value of the protein with another modified peptide (for example, peptide B), this protein will be considered a significantly enriched protein for modified peptide A, otherwise it will be defined as a protein enriched for both modified peptide (A and B).

Co-immunoprecipitation

Cells were collected and disrupted using IP lysis buffer (25 mM Tris, pH 7.4, 150 mM NaCl, 0.5% NP-40, 5% Glycerol, 1mM EDTA) containing 1 mM PMSF and a protease inhibitor cocktail (Roche), followed by sonication (High power, 30 s sonication and 30 s rest). A fraction of the lysate was reserved as an input reference. Simultaneously, Protein A/G beads were incubated with either 4 μg of specific antibody or anti-IgG for 4 h at 4 °C and then washed three times with PBS/BSA. The remaining lysate was subsequently combined with the antibody-bound Protein A/G beads and incubated overnight at 4 °C on a rotating platform. Afterward, the beads were washed four times with wash buffer (50 mM Tris, pH 7.4, 300 mM NaCl, 1% NP-40, 0.5 mM PMSF, protease inhibitor cocktail) at 4 °C. After discarding the supernatant, the beads were resuspended in 40 μL 1× SDS loading buffer and heated at 100 °C for 10 min, followed by western blot analysis. Images were taken by a Chemiluminescence image system (Tanon 5200).

Flow cytometry

Cells were washed twice with ice-cold PBS, pelleted by centrifugation, re-suspended, and then incubated on ice for 10 min in pre-cooled fluorescence-activated cell sorting FACS buffer (PBS and 3% FBS) supplemented with 4′,6-diamidino-2-phenylindole (250 ng/sample). d2EGFP fluorescent signal in E4 or 2D10 cells with or without treatment were measured. Cell cycle stage was determined using flow cytometry. Cells were resuspended in 1 mL 70% ethanol (in phosphate-buffered saline; PBS) overnight at 4°C. Cells were collected by centrifugation (500 × g, 5 min, 4°C), washed once in PBS, resuspended in 500 μL PBS containing propidium iodide (5 μg/mL) and RNase A (0.1 mg/mL), incubated in dark for 30min (37°C). Cells were filtered through a 400-mesh screen and examined. All experiments were detected by flow cytometry CytoFlex and analyzed by FlowJo_V10 software.

Luciferase assay

HEK293T cells were seeded in a 48-well cell culture plate. For siRNA transfection induced knockdown of target genes, cells were transfected with siRNA for 6 h, using Lipofectamine 2000 according to the manufacturer's instructions (Life Technologies). The reaction was stopped by changing with fresh medium. 48 h after transfection, cells were transiently co-transfected with pcDNA-Tat (10 ng/well), HIV LTR-Luciferase (50 ng/well) and pTK-Renilla (5 ng/well) vectors. 36 h later, cells were lysed in 100 μL of passive lysis buffer. The firefly and renilla luciferase activity were measured with the Dual-Luciferase Reporter Assay System (Promega). Before comparison between samples, the relative firefly luciferase activity was determined by normalizing its absolute value to that for the Renilla activity. The siRNA or shRNA induced alteration of the luciferase activity were calculated as the fold change of Luciferase/Renilla ratio for the treatment group compared to that of the untreated control. In the dual luciferase assays for mutant DCAF1 expressing cells, doxycycline (DOX)-induced ablation of *DCAF1* gene was performed two days before co-transfection of the DCAF1 expression vector (wild-type or mutants, 250 ng/well) and the Tat/Luciferase/Renilla plasmid mixtures. Three independent transfection experiments were performed to guarantee reproducibility, each of which was performed with three technical repeats.

Chromatin immunoprecipitation

ChIP assays were carried out following protocol.[73] In brief, 1×10^7 cells were cross-linked for 10 min at room temperature with 1% formaldehyde and then quenched with 0.125 M glycine for 15 min at room temperature. Cells were washed three times in cold PBS before being resuspended in cell lysis buffer (10 mM Tris-HCl pH 8.0, 10 mM NaCl, 0.5% NP-40 and 1× protease inhibitor cocktail). Nuclei were pelleted at 600g for 5 min at 4°C and resuspended in a nuclei lysis buffer (50 mM Tris-HCl pH 8.0, 10 mM EDTA, 1% SDS and 1× protease inhibitor cocktail) and then incubated on ice for 10 min. Sonication was used to shear chromatin DNA to a size of 100–600 bp and 5% of nuclear lysate was saved as input control, 95% of nuclear lysate diluted in the final concentration of 1% Triton X-100, 0.1% sodium deoxycholate and 1× proteinase inhibitor cocktail and was subjected to immunoprecipitation with antibody coupled beads. After immunoprecipitation, beads were washed in low salt buffer (20 mM Tris-HCl pH 8.0, 150 mM NaCl, 2 mM EDTA, 0.1% SDS, and 1% Triton X-100, 1×protease inhibitor cocktail), high salt (20 mM Tris-HCl pH 8.0, 500 mM NaCl, 2 mM EDTA, 0.1% SDS, and 1% Triton X-100, 1×protease inhibitor cocktail), LiCl buffer (10 mM Tris-HCl pH 8.0, 0.25 M LiCl, 1% NP-40, and 1% sodium deoxycholate), and TE (Tris EDTA) buffer. Beads were eluted elution buffer and treated with RNase A at 37°C for 30 min. Cross-linking was reversed, and proteins were degraded by adding proteinase K and incubated at 55°C for 4 h. Eluted DNA was purified and used for qPCR analysis.

HIV-1 reactivation in healthy donors' primary CD4$^+$ T cells

We obtained isolated primary CD4$^+$ T cells from two healthy donors (Milestone Biological Science & Technology Co., Ltd). Isolated CD4$^+$ T cells were seeded in a 96-well flat-bottom plate at a density of 3×10^6 per well in 150 μL of complete growth medium. CD4$^+$ T cells were activated for 48 h with 200 IU IL-2 and ImmunoCult Human CD3/CD28 T cell Activator (STEMCELL Technologies, 10791), and then transduced with pseudotyped HIV-$1_{NL-3/Luciferase}$ viruses. After that, culture the cells until they return to a resting state. To facilitate experimental manipulation in primary CD4$^+$ T cells, we constructed constitutive plasmids pLVX-shDOT1L-1/shDOT1L-2, pLVX-shDCAF1-1/shDCAF1-2 and pLVX-shNC. The second generation lentivirus packaging system was used for generate lentivirus. On day 10, cells were infected with either the shDOT1L or shDCAF1 lentivirus. After 10 h, 2 μg/mL puromycin was used to separate the infected and uninfected CD4$^+$ T cells. Two days later, either TNFα (10 ng/mL) or Prostratin (0.5 μM, 16 h) were used to activate latently infected CD4$^+$ T cells. Luciferase activity and HIV-1 gag mRNA expression were detected using the Cytation3 microplate reader (BioTek) and CFX connect Real-Time PCR detection System (Bio-Rad) instruments.

RNA sequencing

Total RNA was isolated using TRIzol Reagent according to the manufacturer's instructions. RNA-seq library was constructed with MGIEasy RNA Library Prep kit (Cat. No. 1000006383). Briefly, mRNA was captured by adding VAHTS mRNA capture beads to a total of 200 ng RNA, and fragmented to around 250 bp in fragmentation buffer at 87°C for 6 min. Then, reverse transcription mixture and second strand synthesis mixture were successively added to the fragmentation product to generate first strand and second strand of cDNA. The double strand cDNA was purified, fragmented, end-repaired, adapter-ligated and amplified according to the protocol provided by the manufacturer. The yield was circularized to prepare single-strand DNA circle (ssDNA circle) after passing the quality control by Qubit 4.0 Fluorometer (Invitrogen) for concentration measurement and HS DNA chip bioanalyzer (Agilent) for size distribution analysis. ssDNA circle was amplified to generate DNA nanoballs (DNBs) by rolling circle replication to strengthen the fluorescent signals. Then, the DNBs were loaded onto the flowcell, and data of pair-end reads of 100 bp were generated by the DNBSEQ-T1 platform.

RNA-sequencing analysis

The differentially expressed genes (DEGs) between vehicle (DMSO) and EPZ5676-treated cells were detected by the DESeq2 package, based on the analysis criteria of $\geq$ 2-fold change in expression and a false discovery rate of 0.05. The Gene Ontology (GO) analysis of DEGs was performed by clusterProfiler package.

RT-qPCR analysis

For RNA extraction, cell pellets were resuspended in 1 mL of TRIzol reagent (Invitrogen) and the RNA was purified as recommended by the manufacturer. Reverse transcription was performed using the HiScript II Q RT SuperMix for qPCR (+gDNA wiper, R223-01) from Vazyme. PCR was performed using SYBR green PCR master mix (Vazyme, q311) and specific primers.

Confocal immunofluorescence microscopy

For immunofluorescence staining, after cell density reaches a density of 85%, remove the culture medium, wash the cells with PBS, add 4% paraformaldehyde, and shake at room temperature for 15 min to fix the cells. Next, remove the fixative and add an equal volume of Triton X-100 containing 0.5% PBS, penetrate the cells for 5 min, and then remove the fixative. Add blocking solution containing 1% BSA in PBST, block at room temperature for 1 h. Followed by, the cells were then stained for 2 h at room temperature with α-p65, α-DOT1L or α-HA antibodies and then washed with PBST. Finally, cells were incubated with Alexa Fluor 594-conjugated secondary α-mouse antibody (1:1000 dilution; Invitrogen). Nuclei were stained with DAPI (1 μg/mL in 1× PBS). The images were recorded using the Zeiss Pascal laser scanning confocal microscope (Leica TCS SP8).

QUANTIFICATION AND STATISTICAL ANALYSIS

All data represent the results from three independent experiments. Statistical analyses were performed with Graphpad Prism 8.0 software and presented as mean ± SD. The t test was used for comparison between Two groups, One-way ANOVA was used for comparison between more than two groups, and two-way ANOVA was used for comparison between two conditions. Significant differences were set at $^*p \leq 0.05$, $^{**}p \leq 0.01$, and $^{***}p \leq 0.001$ and ns indicates no significant difference.

Cell Reports, Volume *43*

Supplemental information

DOT1L/H3K79me2 represses HIV-1 reactivation via recruiting DCAF1

Fenfei Liang, Jiaxing Jin, Qiming Li, Jiangkai Duan, Ao Jiang, Xiaoqing Chen, Huichao Geng, Kai Wu, Fei Yu, Xiaolu Zhao, Yu Zhou, Deqing Hu, and Liang Chen

Figure S1.

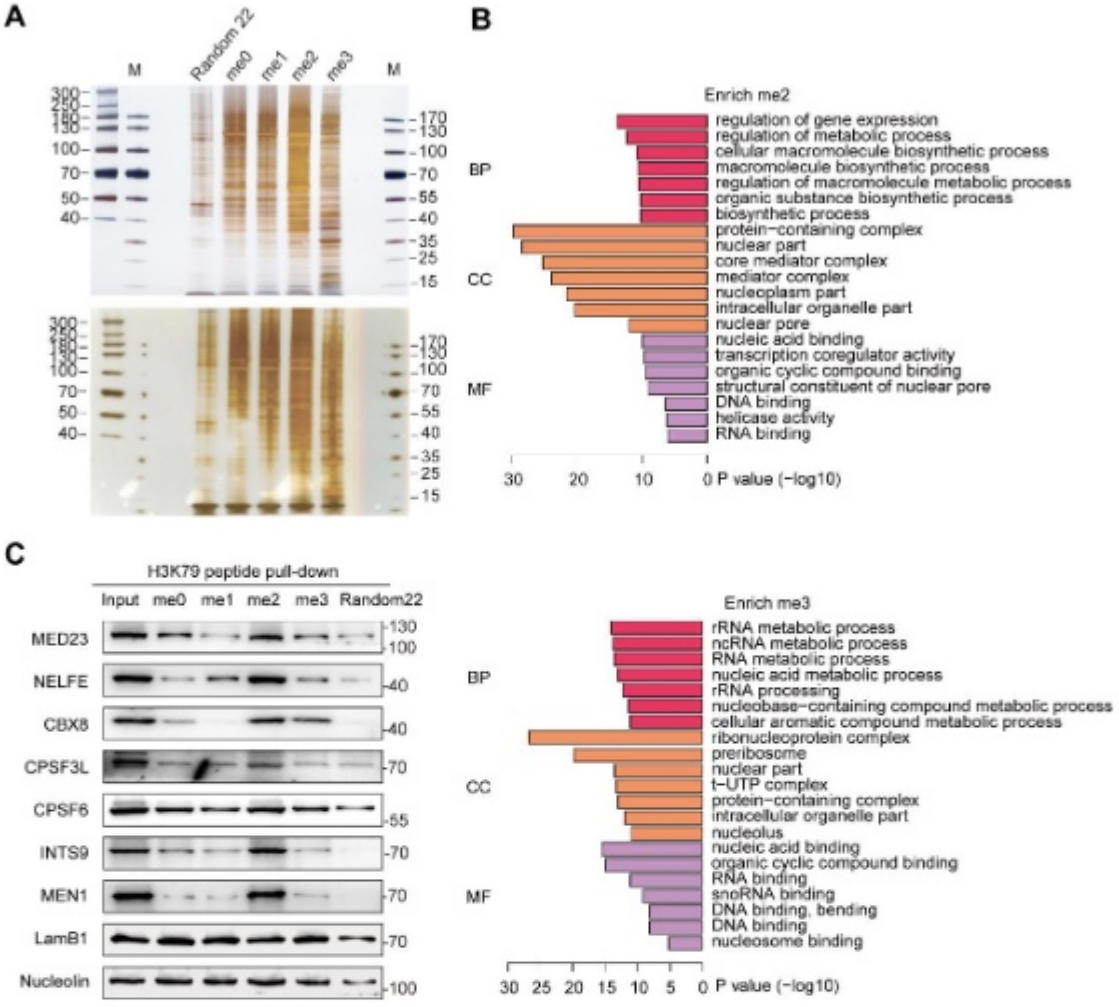

Figure S1. The GO analysis and validation of H3K79me associated proteins. Related to Figure 1.

(A) Two biological replicates of silver staining gel results of peptide pull-down assays.

(B) GO enrichment analyses of H3K79me2 and H3K79me3 associated proteins. MF: Molecular Function, BP: Biological Process, CC: Cellular Component.

(C) In vitro peptide pull-down assays of the nuclear lysate from HEK293T cells with different H3K79 methylated peptides followed by verification of proteins enriched from mass spectrometry data. Random peptide 22 was used as a non-specific binding control. LamB1 and Nucleolin were used as non-specifically associated proteins, and MEN1 was a positive control for H3K79me2 binding.

Figure S2.

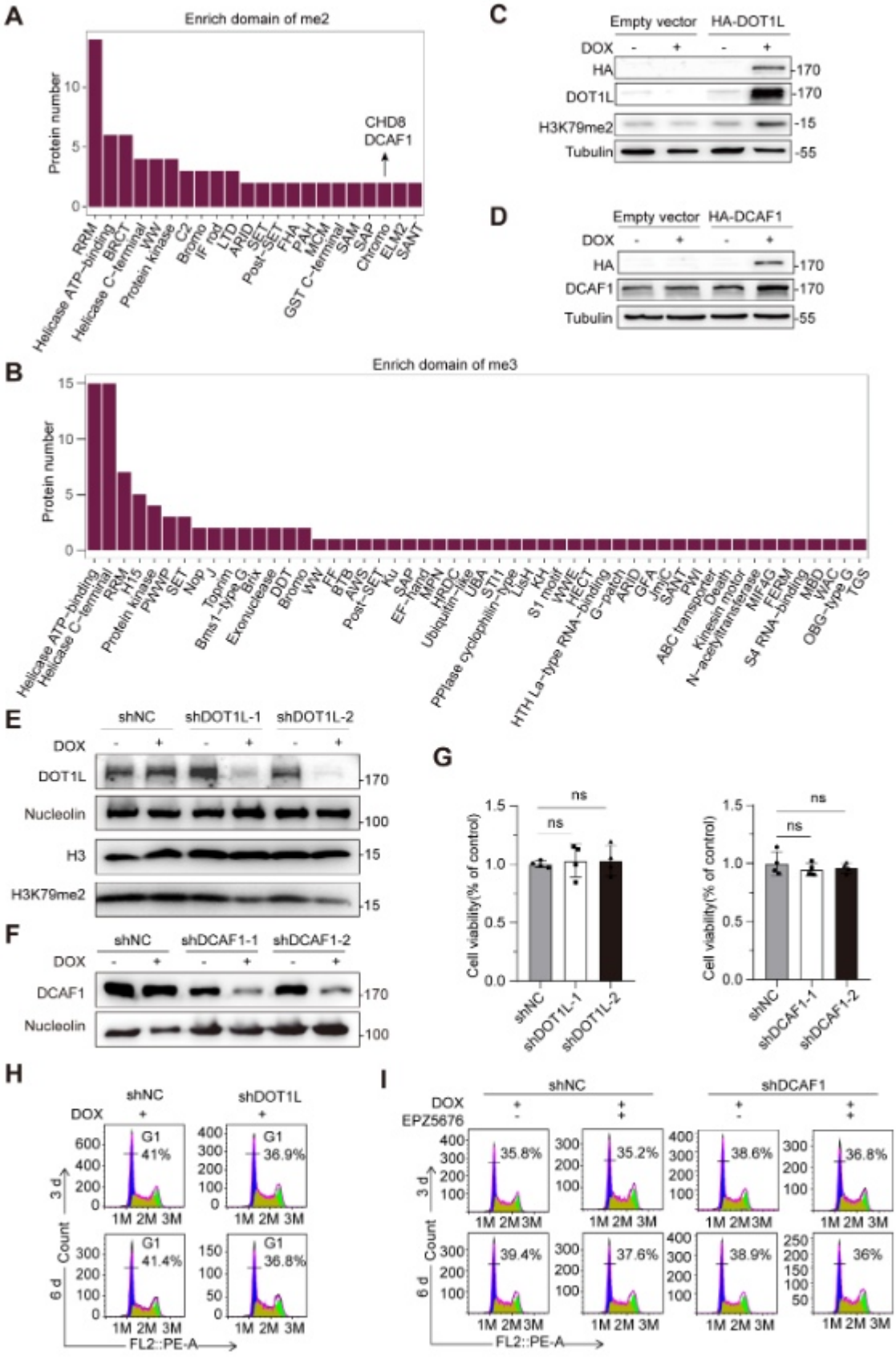

Figure S2. Identification of DCAF1 as an associated protein. Related to Figure 2.

(A and B) Domain enrichment analyses of H3K79me2 (A) and H3K79me3-associated (B) protein. DCAF1 and CHD8 were indicated as chromo domain containing proteins. **(C and D)** Exogenous proteins were verified from HEK293T cell lines overexpressing HA-DOT1L (C) and HA-DCAF1 (D) by Western blot assay. Empty vector: pCW57 vector without insertion of any coding sequence. **(E and F)** HEK293T cells with induced expression of shDOT1L and shDCAF1 were examined by Western blot assay for the protein level of DOT1L and DCAF1. shNC: negative control cells expressing a scramble shRNA sequence. H3 was shown as the loading control for H3K79me2. **(G)** The cell viability examination by CCK8 assays on the HEK293T cell lines exogenously expressing shDOT1L or shDCAF1. Data are presented as means ± SD (n = 4). Statistical significance was determined by the Student's t-test. ns: no significance. **(H)** Cell cycle analysis of HEK293T cells expressing shDOT1L by flow cytometry. **(I)** Cell cycle analysis of HEK293T cells expressing shDCAF1 with or without treatment of EPZ5676 by flow cytometry.

Figure S3.

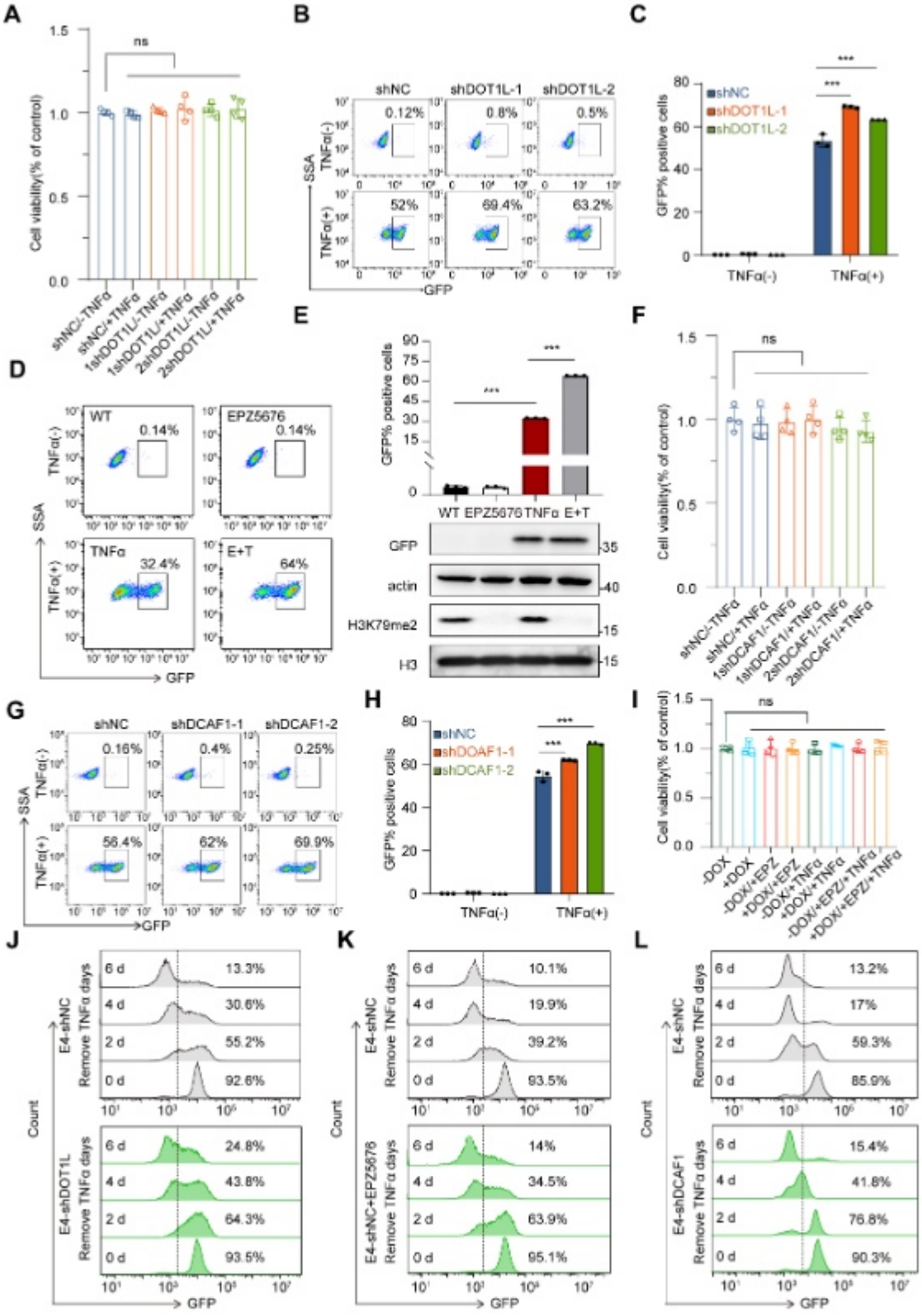

Figure S3. DOT1L/H3K79me2 and DCAF1 repress the latent HIV reactivation. Related to Figure 3.

(A) The cell viability examination by CCK8 assays on the E4 stable cell line expressing shDOT1L with or without TNFα treatment. Data are presented as means ± SD ($n = 4$).

Statistical significance was determined by the Student's t-test. ns: no significance.
(B) Flow cytometry analysis of two shDOT1L 2D10 cell lines at latency and reactivation. Representative results of three technical repeats from at least three reproducible experiments are shown.
(C) Quantification of GFP-positive 2D10 cells expressing shNC and shDOT1L at latency and activation by TNFα. Data are presented as means ± SD ($n = 3$). $***P \leq 0.001$
(D) Flow cytometry analysis of 2D10 cell lines in the absence or presence EPZ5676 at latency and reaction by TNFα. Representative results of three technical repeats from at least three reproducible experiments are shown.
(E) Quantification of GFP-positive 2D10 cells before and after treatment of EPZ5676 and TNFα. The Western blot assay was performed to detect the levels of GFP protein and H3K79me2. Data are presented as means ± SD ($n = 3$).
(F) The cell viability assay on E4 stable cell lines expressing shDCAF1.
(G) Flow cytometry analysis of two 2D10 cell lines expressing shDCAF1 at latency and reactivation by TNFα. Representative results of three technical repeats from at least three reproducible experiments are shown.
(H) Quantification of GFP-positive 2D10 cells expressing shDCAF1 at latency and activation by TNFα. Data are presented as means ± SD ($n = 3$).
(I) The cell viability assay on E4 stable cell lines expressing shDCAF1, with or without the treatment of EPZ5676, TNFα or both.
(J-L) The flow cytometry analysis of GFP-positive E4 cells expressing shDOT1L (J), treated with EPZ5676 (K), or expressing shDCAF1 (L). Cells were treated with TNFα for 24 hours, followed by TNFα withdraw for different time. Corresponding to Figure 3M-O.

Figure S4.

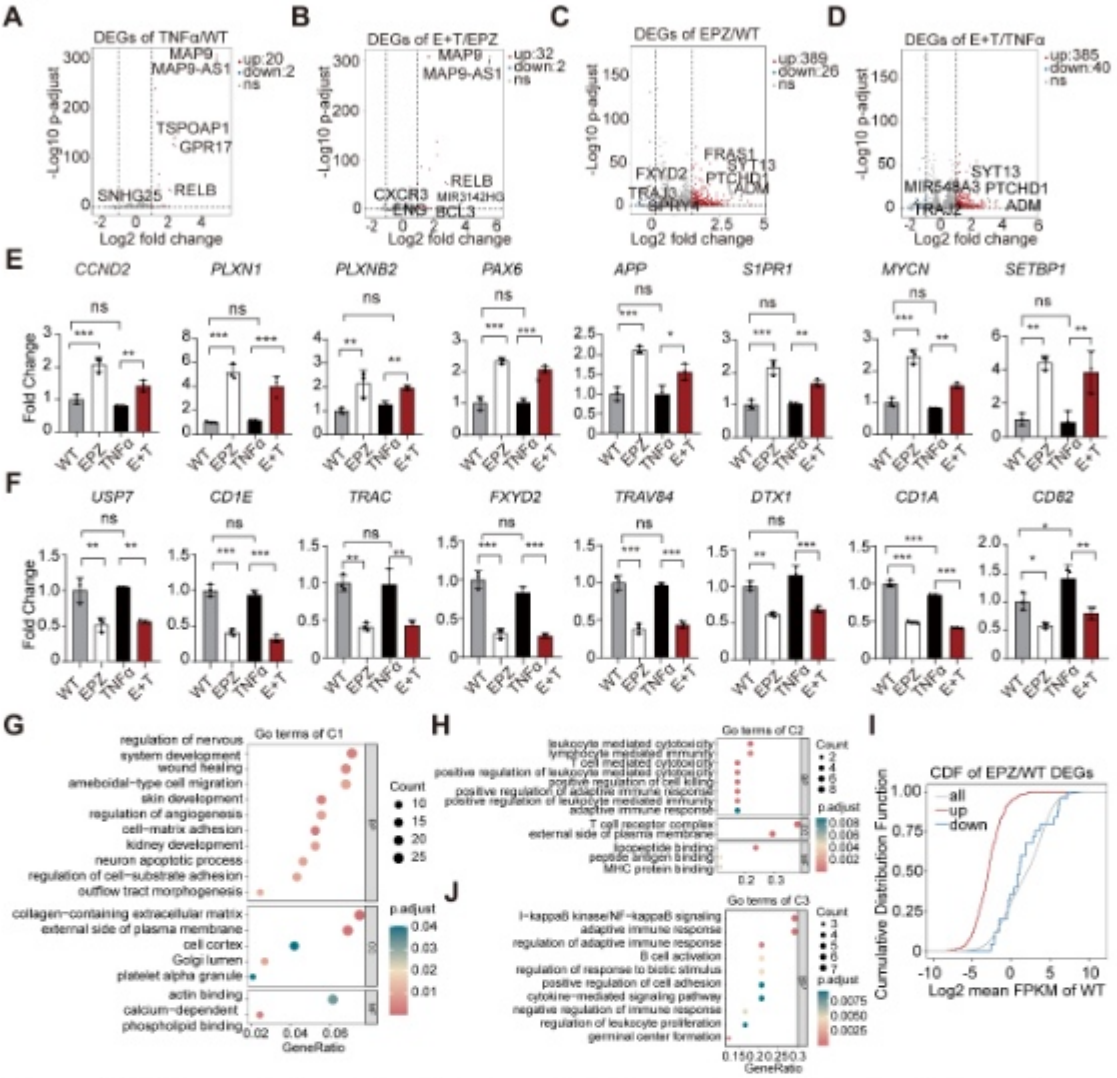

Figure S4. The analysis and validation of RNA-seq data. Related to Figure 4.

(A-D) Volcano plot showing differentially expressed genes in TNFα-treated in comparison to untreated-cells (A), EPZ5676 and TNFα treated- compared to untreated-cells (B), EPZ5676 treated- compared to untreated cells (C), and EPZ5676 and TNFα treated- compared to TNFα treated-cells (D). WT: untreated wild-type cells. EPZ: EPZ5676.

(E) RT-qPCR validation of expression alterations for C1 genes. Data are presented as means ± SD ($n = 3$).

(F) RT-qPCR validation of expression alterations for C2 genes. Data are presented as means ± SD ($n = 3$).

(G-J) GO enrichment analysis of genes from C1 (G), C2 (H), and C3 (J).

(I) The cumulative distribution of the expression levels for upregulated genes (red), downregulated genes (blue), and all genes (gray) in cells treated with EPZ5676 compared to untreated cells. * $P \leq 0.05$, ** $P \leq 0.01$, and *** $P \leq 0.001$, ns: no significance.

Figure S5.

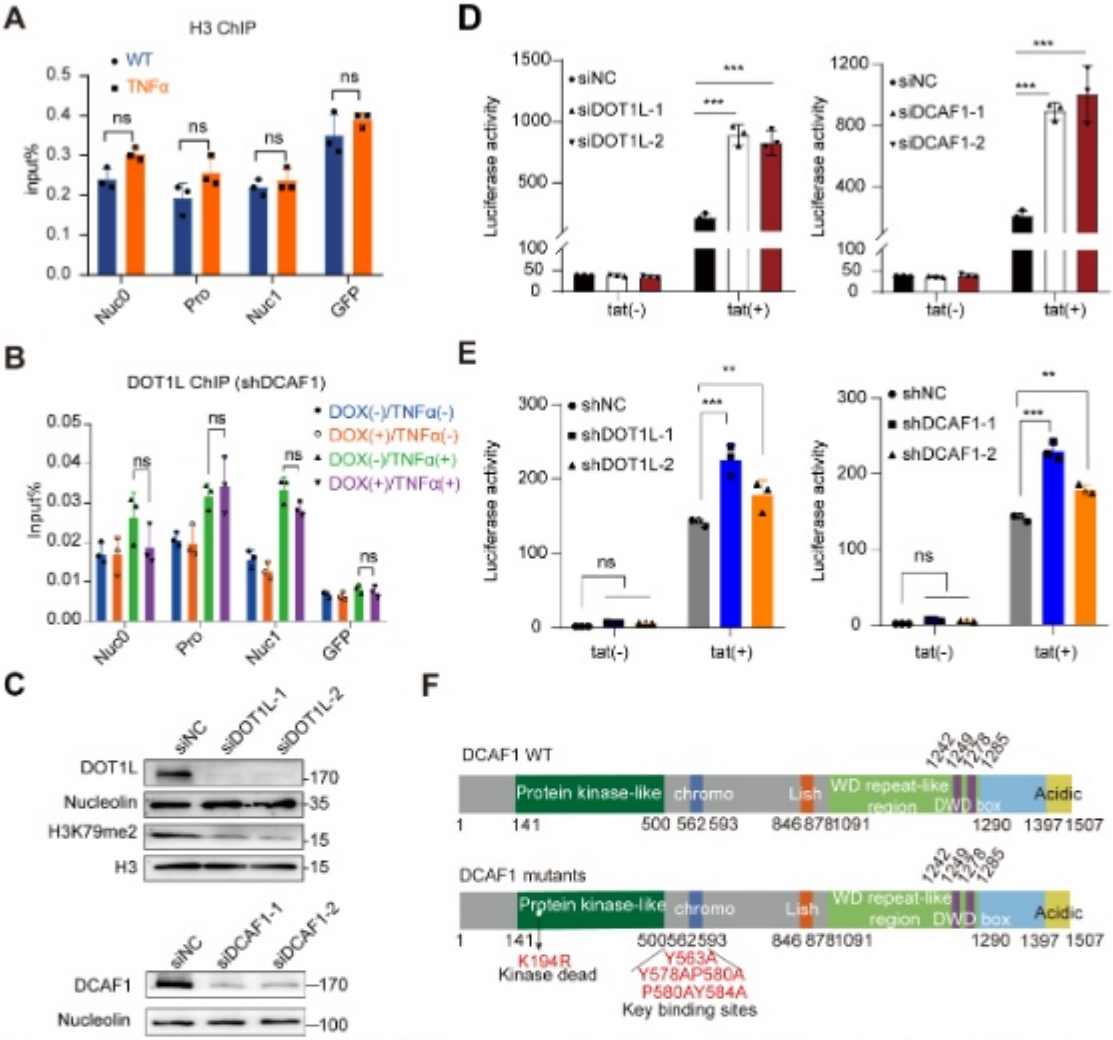

Figure S5. DOT1L and DCAF1 repress Tat-induced HIV activation. Related to Figure 5.

(A) ChIP-qPCR results showing the levels of H3 at the HIV LTR and downstream GFP regions in E4 cells with TNFα treatment. ChIP enrichment values were normalized to input and shown as means ± SD ($n = 3$). Corresponding to Figure 5C.

(B) ChIP-qPCR results showing DOT1L occupancy in E4 cells expressing shDCAF1 with or without TNFα treatment for 12 hours. DOT1L enrichment values were normalized to input and shown as means ± SD ($n = 3$). ns: not significant.

(C) Western blot results showing protein levels of DOT1L and DCAF1 in HEK293T cells transfected with *DOT1L* siRNA (*siDOT1L-1* and *siDOT1L-2*) or *siDCAF1* (*siDCAF1-1* and *siDCAF1-2*).

(D) Luciferase assays results showing HIV-LTR transcriptional activity in HEK293T cells transfected with *siDOT1L* or *siDCAF1*, and pCDNA-tat vector for 12 hours. Luciferase activity was normalized to renilla. Data are presented as mean ± SD ($n = 3$). *** $P \leq 0.001$.

(E) Luciferase assays results showing HIV-LTR transcriptional activity in HEK293T cells expressing shDOT1L or shDCAF1, and pCDNA-tat vector for 12 hours.

Luciferase activity was normalized to renilla. Data are presented as mean ± SD ($n = 3$). ** $P \leq 0.01$, *** $P \leq 0.001$, ns: no significance. **(F)** Schematic domain illustration of full-length DCAF1 protein, individual domains and mutation sites were specified.

Figure S6

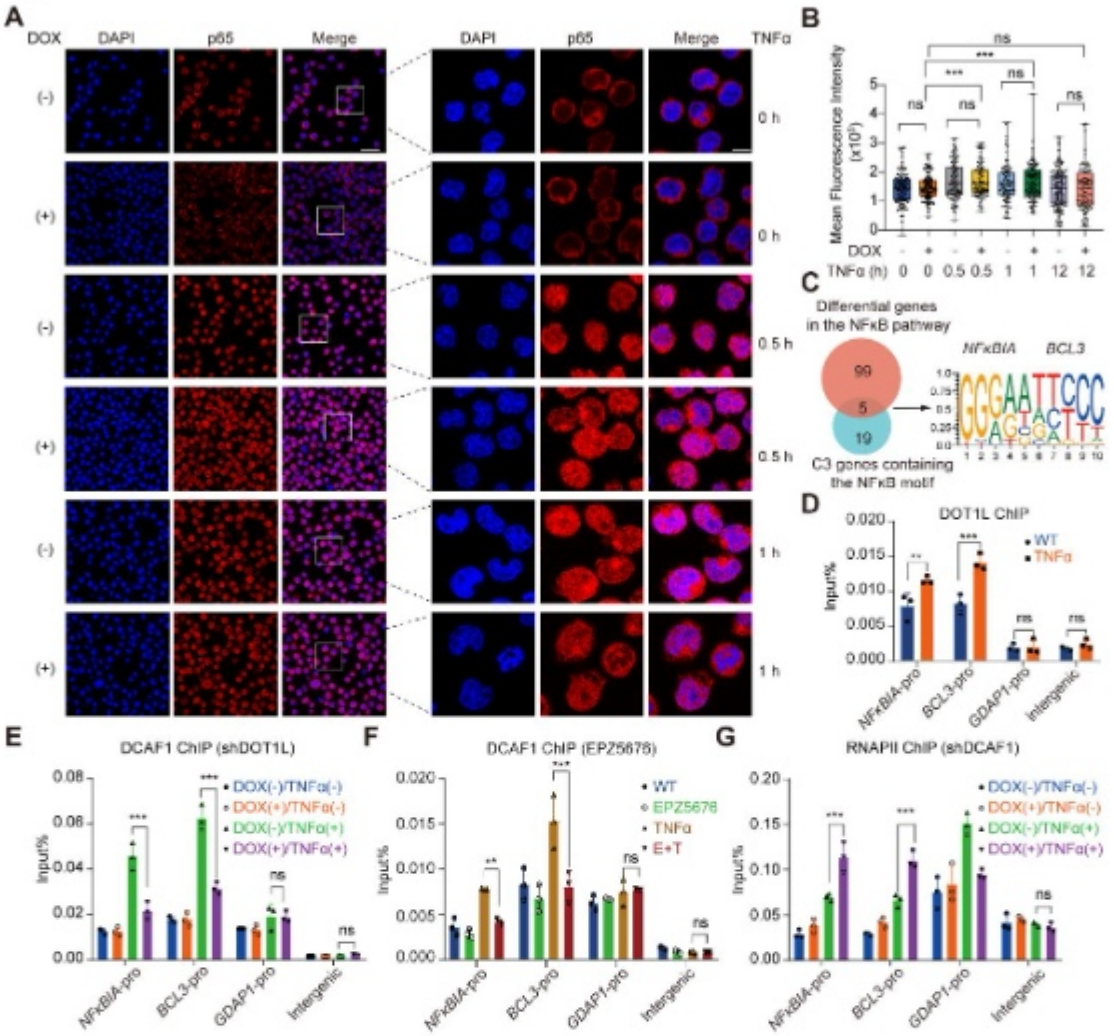

Figure S6. DOT1L and DCAF1 repress transcription of C3 genes induced by TNFα. Related to Figure 6.

(A) Immunofluorescence staining results of p65 in E4 cells expressing shDCAF1 with or without TNFα treatment for 0.5 and 1 hours (left) and representative zoom-in area from the rectangle (right). Scale bar: 25 μm (left); Scale bar: 7.5 μm (right). DAPI (blue), p65 (red).

(B) Quantification of p65 nuclear translocation as a ratio of nucleus and cytoplasm signals from the immunofluorescence staining results. A total of 100 cells were scored and plotted in a box plot. The line corresponds to the median and the box boundaries to the interquartile range (IDR), respectively. Whiskers include all points.

(C) Venn diagram showing shared genes between 24 genes in C3 that contain the NF-κB binding motif and 104 differentially expressed genes in the NF-κB pathway predicted by JASPAR. Five genes, including *NFκBIA* and *BCL3* were shown with the enriched NF-κB binding motif.

(D) ChIP-qPCR results of DOT1L occupancy at the promoters of two NF-κB_target genes from C3 in E4 cells with or without TNFα treatment for 12 hours. The promoter of GDAP1 and a randomly picked intergenic region were included in the assay as non-specific controls. Data were normalized to input and shown as means ± SD ($n = 3$).

(E and F) ChIP-qPCR results of the DCAF1 occupancy at the promoters of two NF-κB target genes in E4 cells expressing shDOT1L, with or without the TNFα treatment (E), and in cells treated with EPZ5676, TNFα or both (F). Data were normalized to input and shown as means ± SD ($n = 3$).

(G) ChIP-qPCR results of total RNAPII distribution at the promoters of two NF-κB target genes in E4 cells expressing shDCAF1 with or without the TNFα treatment (G). Data were normalized to input and shown as means ± SD ($n = 3$). * $P \leq 0.05$, ** $P \leq 0.01$, and *** $P \leq 0.001$.

Figure S7.

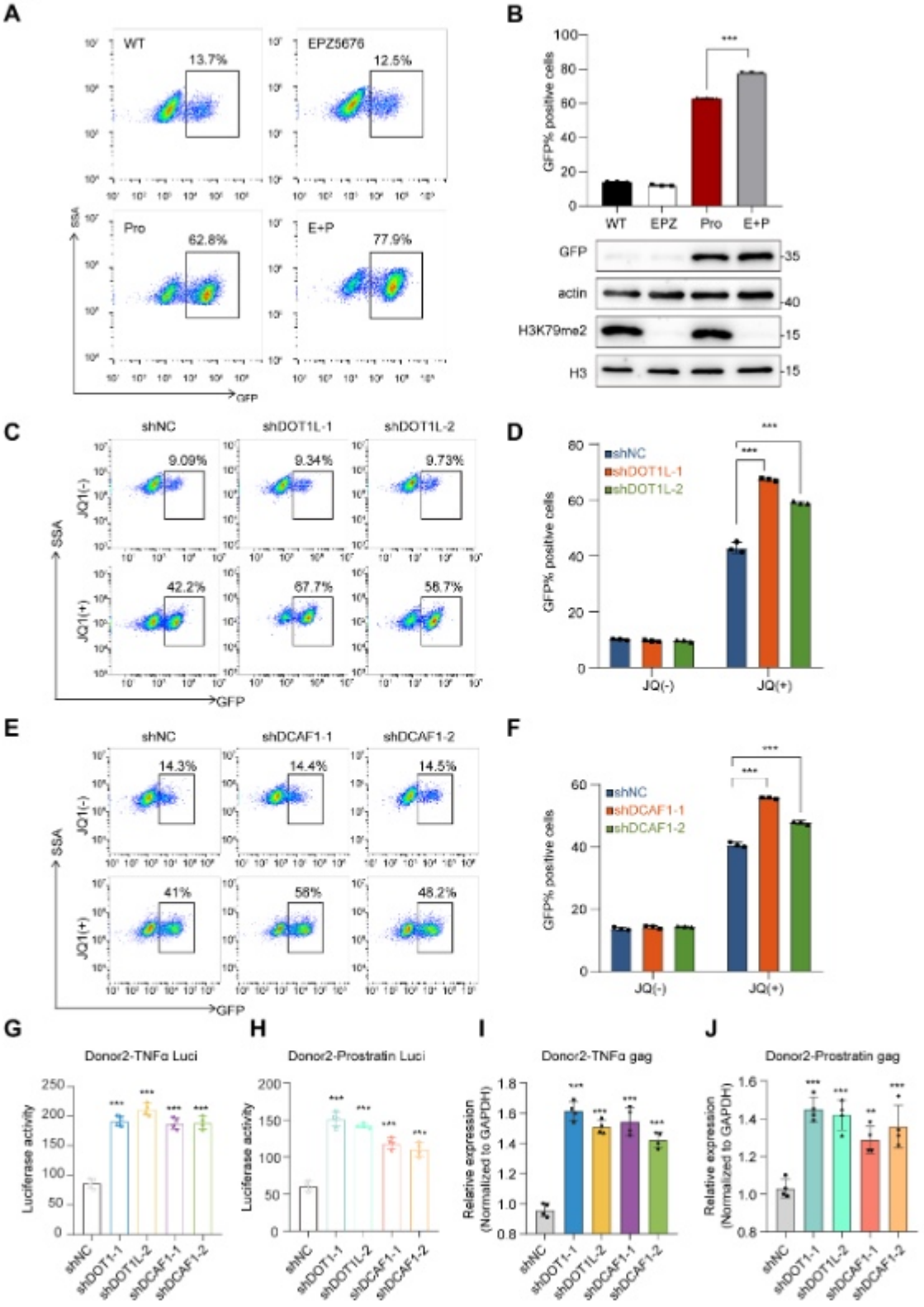

Figure S7. The **HIV-1 reactivation in primary CD4⁺ T cells expressing shDOT1L or shDCAF1 by TNFα or LRA. Related to Figure 7.**

(A) The flow cytometry analysis of E4 cell lines before and after treatment of EPZ5676 and Prostratin. Representative results of three technical repeats from at least three reproducible experiments were shown.

(B) Quantification of GFP-positive E4 cells before and after the treatment of EPZ5676 and Prostratin. The Western blot was performed to detect the levels of GFP protein and H3K79me2. Data are presented as means ± SD ($n = 3$).

(C and D) The flow cytometry assay (C) and quantification (D) showing the percentages of GFP-positive E4 cells expressing shNC, shDOT1L-1 or shDOT1L-2 at latency or upon reactivation by JQ1 treatment.

(E and F) The flow cytometry assay (E) and quantification (F) showing the percentages of GFP-positive E4 cells expressing shNC, shDCAF1-1 or shDCAF1-2 at latency or upon reactivation by JQ1 treatment.

(G-J) Luciferase activity (G and H) and HIV-1 gag mRNA expression level (I and J) detected upon the treatment of TNFα or Prostratin in HIV-infected primary $CD4^+$ T cells from Donor 2 expressing shDOT1L or shDCAF1. Data were normalized to shNC and shown as means ± SD ($n = 4$). ** $P \leq 0.01$, and *** $P \leq 0.001$.

157 **Table S1. List of different methylated binding proteins of H3K79. Related to**
158 **Figure 1.**
159 **Table S2. List of genes containing NF-κB binding sites in the C3 cluster genes.**
160 **Related to Figure 6.**
161 **Table S3. Information of qPCR primers in this paper. Related to Figure 4-6.**